UNIVERSIDAD DE SANTIAGO DE CHILE

FACULTAD DE CIENCIA

Departamento de Física

Van der Waals interaction between Rydberg atoms and polar molecules.

Vanessa Carolina Olaya Agudelo

Profesor Guía:

Felipe Herrera Urbina

Tesis para optar al grado de Magister en Ciencia con Mención en Física.

Santiago – Chile

2019

Resumen

En esta tesis, estudiamos la interacción de largo alcance entre átomos alcalinos de Rydberg con estructura fina (n^2l_j; $l \leq 2$, $15 \leq n \leq 150$) y moléculas alcalinas heteronucleares en el estado base electrónico y rovibracional ($X^1\Sigma^+$; $v = 0$, $J = 0$). Utilizando teoría de perturbaciones para la expansión multipolar en coordenadas esféricas para el potencial de largo alcance, calculamos los coeficientes de dispersión C_6 asociados a la interacción entre pares átomo-molécula que involucran átomos de ^{133}Cs y ^{85}Rb interactuando con moléculas de KRb, LiCs, LiRb, and RbCs. Los coeficientes de dispersión C_6 dependen de la función de polarizabilidad atómica y molecular de los estados de las partículas interactuantes. La magnitud y naturaleza de la interacción es altamente dependiente del estado de Rydberg y puede ser ajustado con precisión a un polinomio $\mathcal{O}(n^7)$ para un rango de números cuánticos principales $40 \leq n \leq 150$. Para todos los pares átomo-molécula considerados, los estados de Rydberg con $l = 0, 1$ tiene interacciones atractivas, mientras que para algunos pares interactuantes con $l = 2$, la interacción resulta ser repulsiva. La energía de interacción a distancias mayores al radio de LeRoy escala como n^{-5} para $n > 40$. Para valores intermedios $n \lesssim 40$, la energía de interacción tanto atractiva como repulsiva está en el orden de los $10-1000\,\mu$K para casos específicos. La exactitud de los coeficientes C_6 calculados está limitada por la calidad de los defectos cuánticos atómicos, con errores relativos estimados no mayores a 1% en promedio.

Palabras claves: Interacción de van der Waals, átomos de Rydberg, moléculas diatómicas.

Abstract

In this thesis, we study the long-range interaction between Rydberg alkali-metal atoms with fine structure (n^2l_j; $l \leq 2$, $15 \leq n \leq 150$) and heteronuclear alkali-metal dimers in the electronic and rovibrational ground state ($X^1\Sigma^+$; $v = 0$, $J = 0$). Using perturbation theory for the multipolar expansion in spherical coordinates of the long-range potential, we compute the associated C_6 dispersion coefficients of atom-molecule pairs involving ^{133}Cs and ^{85}Rb atoms interacting with KRb, LiCs, LiRb, and RbCs molecules. The C_6 dispersion coefficients depend on the atomic and molecular dynamical polarizability of the interacting particles. The magnitude and nature of the interaction is highly dependent on the Rydberg atomic polarizability and can be accurately fitted to a state-dependent polynomial $\mathcal{O}(n^7)$ over the range of principal quantum numbers $40 \leq n \leq 150$. For all atom-molecule pairs considered, Rydberg states n^2S_j and n^2P_j result in attractive $1/R^6$ potentials. In contrast, n^2D_j states give rise to repulsive potentials for specific atom-molecule pairs. The interaction energy at the LeRoy distance approximately scales as n^{-5} for $n > 40$. For intermediate values of $n \lesssim 40$, both repulsive and attractive interaction energies in the order of $10 - 1000\,\mu$K can be achieved with specific atomic and molecular species. The accuracy of the reported C_6 coefficients is limited by the quality of the atomic quantum defects with relative errors $\Delta C_6/C_6$ estimated to be no greater than 1% on average.

Key words: van der Waals interaction, Rydberg atoms, diatomic molecules.

Dedicada a *Juan Manuel Olaya Agudelo*

Acknowledgement

This research has been supported by Fondecyt Regular Grant No. 1181743 and Iniciativa Científica Milenio (ICM) through the Millennium Institute for Research in Optics (MIRO).

Publication

Part of the work presented in this Thesis is published as:

V. Olaya, J. Pérez-Ríos, F. Herrera, C_6 coefficients for interacting Rydberg atoms and alkali-metal dimers, Phys. Rev. A 101, 032705 (2020).

Contents

List of Tables

List of Figures

Introduction

Long-range forces arise from the interaction between well-defined charge distributions at distances between tens to thousands of Bohr radii. These charge distributions can correspond to atoms, molecules, or any other polarizable particle. The interactions energies are small compared with the internal energy of each interacting particle. Therefore, they must be treated pertubatively and can be relevant in the dynamics of ultracold gases and ultracold collisions processes.

In order to study intermolecular potentials in materials, experimental methods such as spectroscopy, scattering and crystallography have been used. To model the intermolecular potential energy, general expressions have been developed. One example is the well-known Lennard-Jones potential [Jones and Chapman, 1924]

$$V_{LJ} = 4\epsilon \left[\left(\frac{R_0}{R} \right)^{12} - \left(\frac{R_0}{R} \right)^{6} \right], \tag{1}$$

where ϵ is the depth of the potential well, R_0 is the distance where $V_{LJ}(R_0) = 0$ and R is the relative distance between the two centers of mass of the system. Figure 1 shows a characteristic Lennard-Jones potential energy curve for a real diatomic molecular system with $\epsilon = -0.00429$ hartrees and $R_0 = 7.05\ a_0$ [Lepers and Dulieu, 2017]. There is also a minimum in Figure 1 at $R = R_m = 7.88\ a_0$, which defines the limit between the repulsive short-range ($R < R_m$) and the attractive long-range ($R > R_m$). The long-range scaling R^6 is characteristic of the *van der Waals* interaction.

The potential curve in Figure 1 allows us to set an energy reference for a system composed of a pair of particles approaching each other from infinity. For a relative kinetic energy on the order of the potential well, the collision processes will be insensitive to the long-range tail. If the relative kinetic energy of the incoming particles is negligible in comparison with the potential well, then the collision dynamics is very sensitive to the long-range tail. The latter case is relevant for the study of few- and many-body physics in the ultracold regime [Lepers and Dulieu, 2017].

At infinite distances, the intermolecular potential energy tends to zero, but we can set a relative distance $R = R_{vdW}$ beyond which we can neglect the potential energy compared with the internal energy of the collision partners. On the other hand, for distances $R < R_{LR}$ short-range processes take place, i.e. the long-range region goes from R_{LR} up to R_{vdW}, where $R_{LR} < R_{vdW}$.

The characteristic distance R_{LR} is known as the LeRoy radius [Le Roy, 1980], which is the min-

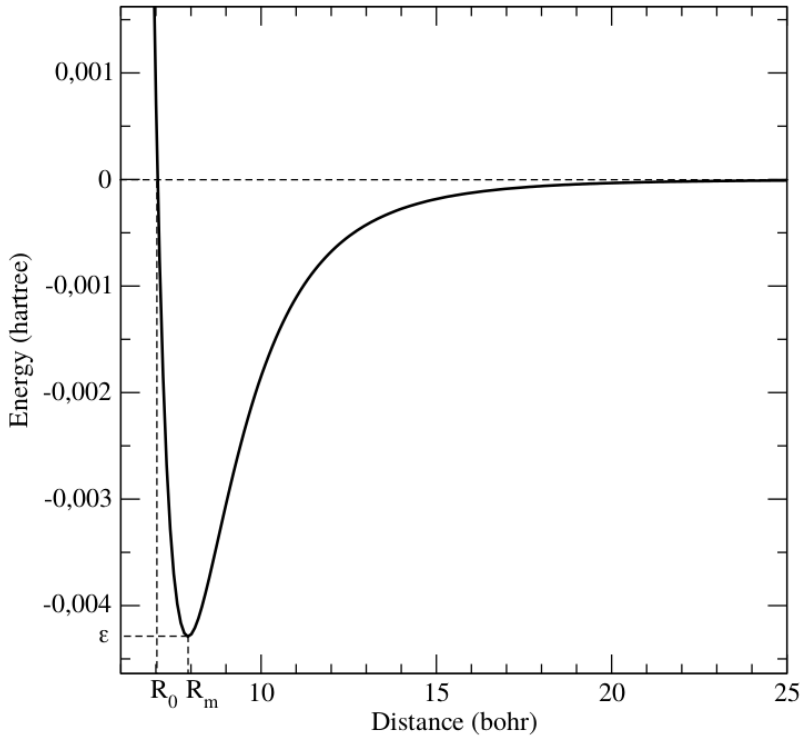

Figure 1: Lennard-Jones potential energy curve according to eq. (1) for a realistic neutral diatomic molecule. Using $\epsilon = -0.00429$ hartrees and $R_0 = 7.05\ a_0$, where the minimum is found at $R = R_m = 7.88\ a_0$. Figure taken from Ref. [Lepers and Dulieu, 2017].

imum distance at which the particles conserve their identity, i.e. their electronic clouds do not overlap. It is given by

$$R_{LR} = 2\left[\sqrt{\langle r_A^2\rangle} + \sqrt{\langle r_B^2\rangle}\right], \tag{2}$$

where r_A and r_B are the mean radii of interacting particles A and B.

The long-range tail varies as C_6/R^6, where C_6 is known as the van der Waals coefficient. The energy and the distance of the van der Waals interaction can also be characterized by [Jones et al., 2006]

$$E_{vdW} = \frac{1}{2}\left(\frac{\hbar^2}{2\mu R_{vdW}^2}\right) \tag{3}$$

and

$$R_{vdR} = \frac{1}{2}\left(\frac{2\mu|C_6|}{\hbar^2}\right)^{1/4}, \tag{4}$$

where μ is the reduced mass of the interacting particles. The van der Waals energy E_{vdW} is commonly larger than the relative kinetic energy of particles in the ultracold regime. For kinetic energies below E_{vdW}, the wavefunction of the colliding particles around R_{vdW} can not be described semi-classically, but purely quantum mechanically [Lepers and Dulieu, 2017].

In general, we denote as van der Waals interaction all those interactions that scale as $1/R^6$. Physically, the origin of the long-range interaction involves permanent or instantaneous inhomogeneities

of the interacting charge distributions, and include the London interactions [London, 1930], Debye interactions [Debye, 1920] and the Keesom interactions [Keesom, 1921].

The van der Waals interaction is not always relevant for gases at room temperature. However, for ultracold gases, the collision dynamics is widely dominated by the long-range tail. Over the last decades, with the development of laser trapping and cooling techniques, the study of long-range interactions for specific systems and their potential application has received special attention in atomic, molecular and optical physics. One of the systems with remarkable applications in a wide variety of areas are Rydberg atoms interacting in the long-range with diatomic molecules. These interacting particles can exchange excitation energies in the microwave regime via Föster processes, which has been proposed as tool for non-destructive detection of molecular states in hybrid molecule-Rydberg systems [Jarisch and Zeppenfeld, 2018, Zeppenfeld, 2017]. Simultaneous trapping of ultracold Rydberg atoms and polar molecules may also be used for direct sympathetic cooling of molecules intro the ultracold regime –a long-standing goal in ultracold physics– through elastic van der Waals atom-molecule collisions [Zhao et al., 2012, Huber and Büchler, 2012]. In comparison with dipole-dipole processes, van der Waals collisions do not require molecules to be confined in low-dimensional traps in the presence of static electric fields for shielding detrimental attractive collisions that lead to trap loss [Ni et al., 2010]. Moreover, van der Waals interactions can be strong even if the relevant transition energies in the collision partners are not resonant, as opposed to Föster processes. Understanding the feasibility of the promising applications of molecule-Rydberg systems thus requires an accurate knowledge of the van der Waals interaction potentials.

In this thesis, we consider atom-molecule systems at low kinetic energies. We focus on alkali-atoms in Rydberg states and polar diatomic molecules in their electronic and rovibrational ground state. Rydberg atoms have exaggerated properties such as orbital sizes of thousands of Bohr radii, long radiative lifetime exceeding microseconds and are extremely sensitive to static electric fields. On the other hand, diatomic molecules have been widely studied and are well characterized and understood in different regimes. At low temperatures, it is possible to prepare atoms and molecules in well-defined quantum states.

The long-range interaction potential of the molecule-Rydberg system is treated perturbatively in comparison with the energy of the Rydberg atom (including the spin-orbit coupling) and the rotational energy of the molecule. Thus, the potential is written as an expansion of the form $V(R) = \sum_n C_n/R^n$, with $n \geq 3$. Since we consider atom-molecule interactions for molecules in their rovibrational ground state, the lowest non-vanishing van der Waals coefficient is found to be C_6 [Lepers and Dulieu, 2011, Lepers et al., 2011, Lepers et al., 2010].

We compute a large set of van der Waals C_6 coefficients that determine the long-range interaction between selected heteronuclear alkali-metal dimers (LiCs, RbCs, LiRb and KRb) in their electronic and rovibrational ground state ($^1\Sigma^+, v = 0, J = 0$) with ^{85}Rb and ^{133}Cs atoms in Rydberg states n^2l_j with $15 \leq n \leq 150$. n is the atomic principal quantum number, l is the atomic orbital angular momentum, j is the total electronic angular momentum, v the vibrational quantum number of the molecule and J is the rotational angular momentum. We focus on molecular [Ni et al., 2008, Blasing et al., 2016, Molony et al., 2014, Deiglmayr et al., 2008b] and Rydberg

atom species [Bellos et al., 2013, Booth et al., 2015] that are experimentally relevant.

The rest of the thesis is organized as follows: in Chapter 1, we describe the theoretical treatment of the Rydberg wavefunctions and compute numerically the atomic dynamical polarizabilities for Rubidium and Cesium atoms in Rydberg states. An overview of the closed-shell diatomic molecules is given in Chapter 2, where we use the Born-Oppenheimer approximation, the adiabatic approximation and the rigid rotor model to obtain the molecular wavefunctions, energies and the dynamical polarizability of ground state alkali-molecules. Chapter 3 is dedicated to the long-range interaction between Rydberg atoms and molecules. We use the multipolar expansion in spherical coordinates of the long-range interaction, together with pertubation theory, to treat this interaction potential and write it in terms of the atomic and molecular dynamical polarizability functions at imaginary frequencies. We also present the scaling of the C_6 coefficients with the atomic principal quantum number and the effect on the interaction of the molecular dipole moment. Finally, in Chapter 3.3.6 we summarize our work and discuss the envisioned applications of our results.

Chapter 1

Alkali-Metal Rydberg Atoms

Atomic Rydberg states [Gallagher, 1994] are highly excited electronic states with a high principal quantum number n. They were predicted at the end of 19th century for the Balmer's wavelength formula for atomic hydrogen [White, 1934]

$$\lambda = \frac{bn^2}{n^2 - 4}, \tag{1.1}$$

where $b = 3645.6$ Å and the wavelegths are given for transitions from $n = 2$ to atomic states with higher principal quantum number. The inverse of eq. (1.1) gives the energy difference between the states, in frequency units

$$\nu = \frac{1}{4b}\left(\frac{1}{4} - \frac{1}{n^2}\right). \tag{1.2}$$

Hydrogen was the first atom to be quantitatively understood. Liveing [Liveing and Dewar, 1879] made important contributions to atomic spectroscopy by observing the spectral lines of sodium. After Liveing and Dewar, Rydberg worked with alkali atoms and classified their spectral lines into sharp, principal and diffuse [Rydberg, 1890] indentifying spectral series with common lower level but upper level in be ns, np and nd states. The frequencies for each series could be expressed as

$$\nu_i = \nu_{\infty i} - \frac{R_y}{(n - \delta_i)^2}, \tag{1.3}$$

with $i = s, p, d$ where $\nu_{\infty i}$ are constants and δ_i are the so-called quantum defects of the sharp, principal and diffuse series. R_y is the well-known universal Rydberg constant with a value equal to 109721.6 cm^{-1}.

It was not until Bohr's model [White, 1934] of the hydrogen atom that the meaning of a high n value became clear. For an electron moving in a circular orbit around the atomic core, the assumtion that the angular momentum was quantized in integral units of $\hbar = h/2\pi$ (h is the Plank's constant), along with the observation that the electron does not continuously radiate around a classical orbit,

but has well defined energies, allowed Bohr to define and orbital radius given by

$$r_n = \frac{4\pi\varepsilon_0\hbar^2 n^2}{Ze^2 m}, \tag{1.4}$$

where ε is the vacuum electric permittivity, Z is the atomic number of the atom, e is the electric change of the electron and m the electron mass. Equation (1.4) showed how the orbital radius increased with the principal quantum number n. The energy W of the state thus decreases with n as

$$W = -\frac{Z^2 e^4 m}{32\pi^2\varepsilon^2\hbar^2 n^2}. \tag{1.5}$$

The energy difference between two atomic states with principal quantum numbers n_1 and n_2 is given by

$$\delta W = W_2 - W_1 = -\frac{Z^2 e^4 m}{32\pi^2\varepsilon^2\hbar^2}\left(\frac{1}{n_1^2} - \frac{1}{n_2^2}\right), \tag{1.6}$$

where $R_y = \frac{Z^2 e^4 m}{32\pi^2\varepsilon^2\hbar^2}$ is the Rydberg constant.

The energy dependence with the principal quantum number $W \sim 1/n^2$ means that for high n the valence electron is in a loosely bound orbit. This loosely bound electron character of a Rydberg electron confers Rydberg atoms with exotic properties. One of these well-known properties is their mean radius: for the ground state hydrogen atom the mean radius is about $1\ a_0$ with a binding energy of $1\ R_y$, while for $n = 10$ these mean radius is about $100\ a_0$ and has a binding energy of the order $0.01\ R_y$. Another important property is the geometric cross section, which scales as n^4. For ground state atoms the geometric cross section is $1\ a_0^2$, while for $n = 10$ is $10^4\ a_0^2$.

The difference between ground state atoms and Rydberg atoms is highlighted when the atoms are exposed to an external electric field. Rydberg atoms are very sensitive to external perturbations. For eletric fields on the order of 10^6 V/cm [Bethe and Salpeter, 1957], Rydberg atoms can be ionized, while the ground state is barely perturbed by these electric field magnitudes. This sensitivity is due the dipole moment and the polarizability of the Rydberg atoms, which scale as n^2 and n^7, respectively. Also, the diamagnetic energy shifts are considerably large compared to ground states. These shifts depend on the area of the orbit, increasing as n^4. These responses to external fields make the Rydberg atoms an useful platform to study light-matter interaction.

Table 1.1 shows some of the properties of Rydberg atoms with a single Rydberg electron and their scaling with the effective principal quantum number n^*.

The development of atomic theory and high resolution absorption spectroscopy allowed the study of Rydberg atoms in the 1970's. The first studies to Rydberg atoms aimed to demostrate their exotic properties.

Amaldi and Segre [Amaldi and Segrè, 1934] studied the energy shifts of the Rydberg series for K in the presence of a rare atomic gas medium. Since the space between the Rydberg electron and the ionic core is filled with a dielectric medium, red shifts were expected for the atomic transitions. These were observed for K, Ar and He, but for Ne only blue shifts where observed. This observations were latter explained by a theory developed by Fermi [Fermi, 1934], in which the energy shifts come from the short range scattering of the Rydberg electron and the atoms in the gas. In

Property	Formula	x
Binding Energy E_n	$-\frac{R_{Ryd}}{(n^*)^2}$	-2
Energy spacing	$E_n - E_{n-1}$	-3
Orbital radius $\langle r \rangle$	$\frac{1}{2}(3(n^*)^2 - l(l+1))$	2
Geo. cross section	$\pi \langle r \rangle^2$	4
Dipole moment	$\langle nd \vert er \vert nf \rangle$	2
Polarizability	$2\sum_{n'l'm'} \frac{\vert\langle nlm \vert z \vert n'l'm'\rangle\vert^2}{E_{nl} - E_{n'l'}}$	7
Radiative lifetime	$2.09\text{ns}(n^*)^{2.85}$	3
Fine-structure	4.8×10^6 MHz $5/2(n^*)^{-3}$	-3

Table 1.1: Properties of the Rydberg atoms, formula and its scaling power x with the effective principal quantum number n^{*x}. Table taken from Ref. [Singer, 2004].

2000, using the Fermi pseudopotential for the short range scattering in the ultracold regime, C. H. Greene, A. S. Dickinson and H. R. Sadeghpour [Greene et al., 2000] predicted that the oscillatory probability density of the Rydberg electron can create long-range potential wells that are suitable to trap surrouding atoms. Those exotic molecules are known as ultralong-range Rydberg molecules and were observed experimentally in 2009 by V. Bendkowsky et al. [Bendkowsky et al., 2009].

Rydberg atoms have been widely studied at room temperature and the effect of an electrid field in these atoms have been continuously studied and observed due to its potential to create techniques for detection and manupulation of Rydberg atoms. Together with the development of the tunable dye laser [Schäfer, 1990], it was possible to excite a large number of atoms to a well-defined Rydberg level. This method allowed the measuarement of several properties such as collision cross sections, transition energies and radiative lifetimes for low lying Rydberg levels.

The exaggerated response of Rydberg atoms to the radiation field has motivated the use of these atoms for testing the interaction with the vacuum of a resonant cavity [L'Huillier et al., 1982]. In the low frequency regime of high Rydberg state, the wavelengths are sufficiently large to facilitates the design of microwave cavities and the radiative decay rates are also appropriate for the system.

Advances in laser technology, cooling and trapping techniques led to the creation of Rydberg atoms in the ultracold regime. Nowadays it is possible to excite the atoms of an alkali gas into a Rydberg level and trap them with a high density of the order of (10^{14}cm^{-3}) in the μK regime [Liebisch et al., 2016]. Such a high density gas allows the to study of Rydberg-Rydberg interactions [Kamenski et al., 2017], which can be tuned by changing the density of the gas or the principal quantum number of the excited atoms. The Rydberg-Rydberg van der Waals interaction scales as n^{11} and is strong enough to create molecular Rydberg state with bound lengths of the order of thousand of Bohr radii [Samboy et al., 2011].

Quantum information processing is another area in which Rydberg atoms can also be exploited. By using the strong dipole-dipole interactions between Rydberg atoms, fast phase gates have been implemented [Jaksch et al., 2000], where the ground state levels are used to store information, while the Rydberg states that strongly interact create the entangled states. For a short period, the atoms will be decoupled from the environment decreasing the decoherence. For mesoscopic systems, Lukin [Lukin et al., 2001] proposed to forget about the tricky single atom control by us-

ing the *dipole blockade* in which the interaction between excited atoms inhibits several Rydberg exitation in the neighboring atoms.

These application along with the description given in Chapter are some of the applications that show the richness of Rydberg physics. This chapter explains the theoretical treatment used to study Rydberg atoms and elaborates on some of their physical properties that are required to understand the role of Rydberg atoms when they interact with ground state molecules in the long-range regime.

1.1 Rydberg atom wavefunctions

This section discusses the theoretical treatment of the Rydberg alkali-atom wavefunction. We use a hydrogen-like Schrödinger equation to model the electron-core system. We use an effective radial interaction potential $V_l(r)$ (r is the distance between the electron and the ionic core) that accounts for the effect of the inner electrons of the core over the valence electron and behaves as a Coulomb potential at large distances ($r \to \infty$). The Rydberg energies are described using the quantum defects δ_{nlj} and the spin-orbit coupling of the atom is mapped through the quantum defects by adding a dependence of the total angular momentum j. Hyperfine structure is neglected.

The radial Schrödinger equation obtained at the end of the next section is solved numerically using the Numerov algorithm. These numerical wavefunctions allow us to study several properties of Rydberg alkali-atoms.

Atomic units are used throughout this Thesis unless otherwise stated.

1.1.1 Schrödinger equation

We start with the Schrödinger equation of the electron-core system written in terms of the relative distance r and the relative angular orientation (θ, φ),

$$\left[-\frac{\nabla^2}{2\mu} + V_l(r)\right]\Psi(r,\theta,\varphi) = E_{n,l}\Psi(r,\theta,\varphi), \tag{1.7}$$

where $\mu = m_e m_c/(m_e + m_c)$ is the reduced mass, m_c is the mass of the nucleus plus the inner electrons and m_e is the electron mass. $E_{n,l}$ is the energy of the valence electron, which depends on the principal quantum number n and the orbital angular momentum l. The effective interaction potential depends on the orbital angular momentum as well. $\Psi(r,\theta,\phi)$ is the wavefunction of the system.

The ∇^2 operator in spherical coordinates is given by

$$\nabla^2 = \frac{\partial^2}{\partial r^2} + \frac{2}{r}\frac{\partial}{\partial r} + \frac{1}{r^2\sin\theta}\frac{\partial}{\partial\theta}\left(\sin\theta\frac{\partial}{\partial\theta}\right) + \frac{1}{r^2\sin^2\theta}\frac{\partial^2}{\partial\varphi^2}. \tag{1.8}$$

The square of angular momentum operator $\mathbf{l}^2$ can be written in spherical coordinates as

$$\mathbf{l}^2 = \frac{1}{\sin\theta}\frac{\partial}{\partial\theta}\left(\sin\theta\frac{\partial}{\partial\theta}\right) + \frac{1}{\sin^2\theta}\frac{\partial^2}{\partial\varphi^2}. \tag{1.9}$$

Therefore, eq. (1.8) can be written as

$$\nabla^2 = \frac{\partial^2}{\partial r^2} + \frac{2}{r}\frac{\partial}{\partial r} + \frac{1}{r^2}\mathbf{l}^2. \tag{1.10}$$

Inserting eq. (1.10) into the Schrödinger equation (1.7) gives

$$\left[-\frac{1}{2\mu}\left(\frac{\partial^2}{\partial r^2} + \frac{2}{r}\frac{\partial}{\partial r}\right) + \frac{\mathbf{l}^2}{2\mu r^2} + V_l(r)\right]\Psi(r,\theta,\varphi) = E_{n,l}\Psi(r,\theta,\varphi). \tag{1.11}$$

The system wavefunction can be separated into a radial and angular part as $\Psi(r,\theta,\phi) = R(r) \times Y_l^m(\theta,\phi)$, where $Y_l^m(\theta,\phi)$ is the spherical harmonic of order l with component m, explicitly given by

$$Y_l^m(\theta,\phi) = \sqrt{\frac{(2l+1)(l-m)!}{4\pi(l+m)!}}P_l^m(\cos\theta)e^{im\varphi}, \tag{1.12}$$

where P_l^m are the associated Legendre polynomials [Lebedev, 1965]. The angular equation (in units $\hbar = 1$) can be written as $\mathbf{l}^2 Y_l^m = l(l+1)Y_l^m$. The radial equation is thus given by

$$\left(-\frac{1}{2\mu}\left[\frac{d^2}{dr^2} + \frac{2}{r}\frac{d}{dr}\right] + \left[\frac{l(l+1)}{2\mu r^2} + V_l(r) - E_{n,l}\right]\right)R(r) = 0. \tag{1.13}$$

1.1.2 Atomic State notation

For alkali-atoms, we must consider the electronic spin angular momentum $\mathbf{s}$, which is coupled to the orbital angular moment operator $\mathbf{l}$ to form the total angular momentum operator $\mathbf{j} = \mathbf{l}+\mathbf{s}$, which is a vector addition of $\mathbf{l}$ and $\mathbf{s}$ and follows the so-called triangular condition, namely

$$m = m_l + m_s \tag{1.14}$$

and

$$|l-s| \leq j \leq |l+s| \tag{1.15}$$

where m, m_l, m_s are the projection of $\mathbf{j}$, $\mathbf{l}$, $\mathbf{s}$ in the reference frame, respectively, and j, l, s are the magnitude of the corresponding vectors. For the Rydberg alkali-atoms considered in this Thesis (^{133}Cs and ^{85}Rb), the electronic spin is $s = 1/2$.

We will refer to an atomic Rydberg state by their quantum numbers n, l, s, j, m using indistinctly the state notations $|n(ls)jm\rangle$, or $|nljm\rangle$, or $|n^{2s+1}l_j, m\rangle = |n^2 l_j, m\rangle$.

l	r_c	a_1	a_2	a_3	a_4
^{133}Cs, $\alpha_c = 15.6440$					
0	1.92046930	3.49546309	1.47533800	-9.72143084	0.02629242
1	2.13383095	4.69366096	1.71398344	-24.65624280	-0.09543125
2	0.93007296	4.32466196	1.61365288	-6.70128850	-0.74095193
≥ 3	1.99969677	3.01048361	1.40000001	-3.20036138	0.00034538
^{85}Rb, $\alpha_c = 9.0760$					
0	1.66242117	3.69628474	1.64915255	-9.86069196	0.19579987
1	1.50195124	4.44088978	1.92828831	-16.79597770	-0.81633314
2	4.86851938	3.78717363	1.57027864	-11.65588970	0.52942835
≥ 3	4.79831327	2.39848933	1.76810544	-12.07106780	0.77256589

Table 1.2: Core potential parameters a_i, critical penetration radius r_c and core polarizability α_c for Cesium and Rubidium. Parameters taken from Ref. [Marinescu et al., 1994].

1.1.3 Core potential

Marinescu et al. [Marinescu et al., 1994] developed a model that accounts for the penetration and polarization of the atomic core due to the valence electron. For a valence electron with low-lying angular momentum ($l \leq 3$) its orbit is elliptic and can be subjected to an unscreened nuclear charge that has the form of the Coulombic potential at large distances. Explicitly, $V_l(r)$ has the form [Marinescu et al., 1994]

$$V_l(r) = -\frac{Z_{n,l}(r)}{r} - \frac{\alpha_c}{2r^4}\left(1 - e^{-(r/r_c)^6}\right), \tag{1.16}$$

where α_c is the static dipole polarizability of the core, and $r_c \sim \alpha_c^{1/3}$ is the critical penetration radius between the valence electron and the core at which the short range contribution to the effective potential (1.16) is not well defined. The first term is related to the core penetration, similar to the Coulomb potential with an effective charge $Z_{n,l}$ of the core, that is given by

$$Z_{n,l} = 1 + (Z-1)e^{-a_1 r} - r(a_3 + a_4 r)e^{-a_2 r}, \tag{1.17}$$

where Z is the regular nuclear charge of the atom, a_i ($i = 1, ..., 4$) are parameters that depend on the atomic species and on the angular momentum of the valence electron. The parameters a_i are tabulated in Table 1.2 for different alkali-atoms.

The second term in eq. (1.16) accounts for the core polarization due to the electron and describes the long range potential mostly determined by the core polarizability α_c, which depends of number of electrons in the core. This potential was parametrically fitted to one-electron energy level with an accuracy of 10^{-5} and successfully predicted several resonant phenomena observed in alkali-atoms. Figure 1.1 shows the core potential function $V_l(r)$ for Rubidium using the potential parameters of Table 1.2 for $l = 0, 1, 2, 3$. The Coulomb potential tends to zero faster that the effective potential V_l for the same atom.

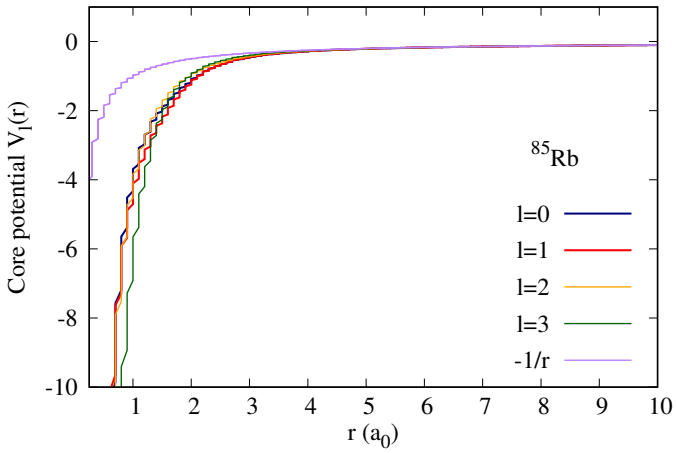

Figure 1.1: Core potential $V_l(r)$ for Rubidium with $l = 0, 1, 2, 3$ using the parameters a_i ($i = 1, 2, 3, 4$) tabulated in Table 1.2. V_l is compared with the Coulomb potential $-1/r$.

1.1.4 Quantum defects

The electrons in the core for alkali-atoms also influence the energy of the valence electron and this is the main difference between hydrogen and alkali-atoms. For the latter, the energy of the valence electron is given by

$$E_{n,l} = -\frac{hcR_\infty}{(n - \delta_{n,l})^2}, \tag{1.18}$$

where $hcR_\infty = 1/2$ is the Rydberg constant in atomic units. As the valence electron is further away from the core, it feels a positive net charge. However, as the electron gets closer, this is not true anymore and the core can be polarized for states with low angular momentum. This phenomenon can be encoded into an effective principal quantum number $n^* = n - \delta_{n,l}$, where $\delta_{n,l}$ is called the quantum defect and has a greater value for lower orbital angular momentum. For $l \geq 3$ the quantum defects are effectively zero, coresponding to a pure Coulombic potential.

The effect of the single-electron spin-orbit potential $V_{so}(r) = (\alpha/r^2)\mathbf{l} \cdot \mathbf{s}$ is negligible on the calculations of the radial wavefunctions ($\alpha \approx 1/137$). Therefore, it is possible to effectively include the spin-orbit interaction by replacing $\delta_{n,l}$ with $\delta_{n,l,j}$ using the extended Rydberg-Ritz formula,

$$\delta_{n,l,j} = a + \frac{b}{(n-a)^2} + \frac{c}{(n-a)^4} + \frac{d}{(n-a)^6} + \frac{e}{(n-a)^8} + \ldots. \tag{1.19}$$

The Rydberg-Ritz coefficients a-e are taken from experimental data. Table 1.3 shows the Rydberg-Ritz coefficients for ^{133}Cs and ^{85}Rb.

Tables 1.4 and 1.5 show the transition energies between different Rydberg states computed using the quantum defects from Table 1.3 for ^{133}Cs and ^{85}Rb, respectively. Our computed energies have an error smaller than 0.1% compared with available experimental data [Deiglmayr et al., 2016, Li et al., 2003].

Figure 1.2 shows the transition energy gaps between atomic states with different angular momen-

l_j	a	b	c	d	n_{min}
		^{133}Cs			
$S_{1/2}$	4.049352(38)	0.238(7)	0.24044	0.12177	6
$P_{1/2}$	3.5916(5)	0.36(1)	0.34284	1.23986	6
$P_{3/2}$	3.5590(7)	0.38(1)	0.28013	1.57631	6
$D_{3/2}$	2.475454(20)	0.010(4)	-0.43324	-0.96555	5
$D_{5/2}$	2.466308(30)	0.015(6)	-0.43674	-0.74442	5
$F_{5/2}$	0.033587	-0.213732	0.70025	-3.66216	4
		^{85}Rb			
$S_{1/2}$	3.1311804(10)	0.1784(6)	-1.8	–	14
$P_{1/2}$	2.6548849(10)	0.2900(6)	-7.9040	116.4373	11
$P_{3/2}$	2.6416737(10)	0.2950(7)	-0.97495	14.6001	13
$D_{3/2}$	1.34809171(40)	-0.60286(26)	-1.50517	-2.4206	4
$D_{5/2}$	1.34646572(30)	-0.59600(18)	-1.50517	-2.4206	4
F_j	0.016312	-0.064007	-0.36005	3.2390	4

Table 1.3: Rydberg-Ritz coefficients for ^{85}Rb and ^{133}Cs. The last column n_{min} is the minimum value of n for which the expansion is estimated to be valid. Data taken from Ref. [Singer, 2004].

$n^2l_j \rightarrow n'^2l'_{j'}$	Ref. [Deiglmayr et al., 2016]	This work
$45^2P_{3/2} \rightarrow 49^2S_{1/2}$	287476.992	287464.770
$59^2P_{3/2} \rightarrow 68^2S_{1/2}$	265898.688	265894.066
$67^2P_{3/2} \rightarrow 81^2S_{1/2}$	261818.142	261815.154
$72^2P_{3/2} \rightarrow 90^2S_{1/2}$	257008.756	257006.406
$59^2P_{3/2} \rightarrow 66^2D_{5/2}$	255306.920	255067.697

Table 1.4: Transition energy in MHz between selected Rydberg states of ^{133}Cs compared with experimental data taken from Ref. [Deiglmayr et al., 2016].

	$n^2S_{1/2} \rightarrow n^2P_{1/2}$		$n^2S_{1/2} \rightarrow n^2P_{3/2}$	
n	Ref. [Li et al., 2003]	This work	Ref. [Li et al., 2003]	This work
27	223664.264	223671.632	–	–
28	197990.586	197996.151	203322.762	203321.703
29	176100.586	176104.837	180848.640	180847.820
30	157322.108	157325.423	161568.406	161567.725
31	141121.445	141124.021	144934.120	144933.648
32	127070.956	127072.994	130507.152	130506.799
33	114825.466	114827.083	117933.187	117932.887
34	104104.194	104105.474	–	–

Table 1.5: Transition energy in MHz between selected Rydberg states of ^{85}Rb compared with experimental data taken from Ref. [Li et al., 2003].

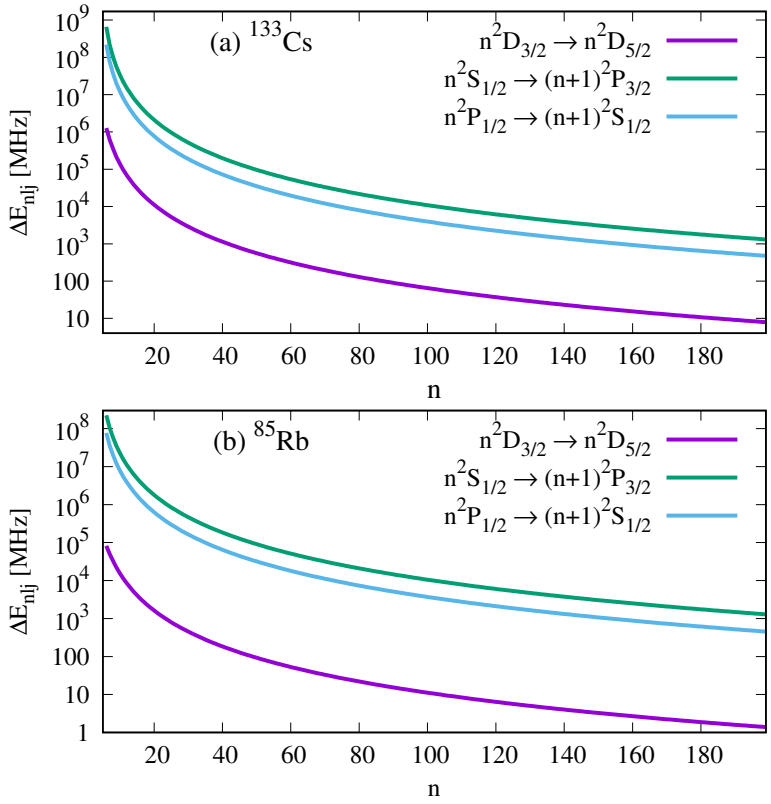

Figure 1.2: Transition energy ΔE_{nlj} between atomic states $n^2D_{3/2} \rightarrow n^2D_{5/2}$, $n^2S_{1/2} \rightarrow (n+1)^2P_{3/2}$ and $n^2P_{1/2} \rightarrow (n+1)^2S_{1/2}$ as a function of the principal quantum number n, for (a)^{133}Cs and (b)^{85}Rb. Logarithmic scale (base 10) is used for ΔE_{nlj}.

tum quantum numbers as a function of n. The smallest energy gap for Rubidium and Cesium is found for the transition $n^2D_{3/2} \rightarrow n^2D_{5/2}$ which range between 1000 to 1 MHz for $n = 20$ to $n = 200$, respectively. For the transition $n^2P_{1/2} \rightarrow (n+1)^2S_{1/2}$ the energy gap is of the order of 10 GHz for $n \sim 71$ in Rb atoms and $n \sim 73$ for Cs.

1.1.5 Radial wavefunction

In order to compute the radial wavefunction of a Rydberg atom, we come back to eq. (1.13) and define the scaled radial function $U(r) = r\ R(r)$ to remove the first derivative, obtaining

$$\frac{d^2U(r)}{dr^2} + \left(2\mu\left[E_{n,l,j} - V_l(r)\right] - \frac{l(l+1)}{r^2}\right) U(r) = 0. \tag{1.20}$$

The radial wavefunction $U(r)$ has stronger oscilations as the radial coordinate r decreases. These oscillations lead to accumulation of errors at small radii. To smoothen these oscilations, the radial Schrödinger equation (1.20) can be rescaled by defining the function $\chi(r) = r^{-1/4}U(r)$ and the radial coordinate as $u = \sqrt{r}$ [Bhatti et al., 1981]. Thus eq. (1.20) becomes

$$\frac{d^2\chi}{du^2} + \left(8\mu u^2\left[E_{n,l,j} - V_l(u)\right] - \frac{4l(l+1)+3/4}{u^2}\right) \chi = 0. \tag{1.21}$$

n	Ref. [Lei et al., 1995]	This work
6	15.7	15.7
10	82.0	82.3
20	458	459
22	589	570
25	758	759
30	1133	1135
35	1584	1585
40	2110	2111
45	2710	2711.5
50	3386	3387
55	4136	4138
60	4961	4963

Table 1.6: Mean radius $\langle r \rangle$ in atomic units (a_0) for Cesium Rydberg atom in a nD state . The values computed numerically in this work (third column) are compared with the results obtained in Ref. [Lei et al., 1995] using the scaling formula $\langle r \rangle = [3(n - \delta_{nl})^2 - l(l+1)]/2$.

n	Ref. [O'Sullivan and Stoicheff, 1986]	This work
15	274(75)	254
20	520(150)	474
25	800(300)	762
30	1200(400)	1118
35	1800(650)	1542
37	1800(800)	1730
40	2100(850)	2033
45	2700(1900)	2593
50	3500(1900)	3220
55	3800(2300)	3914

Table 1.7: Radial integral $\langle n^2 l_j | r | n'^2 l'_{j'} \rangle$ of the atomic transition $n^2D \rightarrow (n+1)^2P$ for Rubidium taken from Ref. [O'Sullivan and Stoicheff, 1986] compared with the values computed in this work using $j = 3/2$. The parenthesis shown in the second column correspond to the experimental error band.

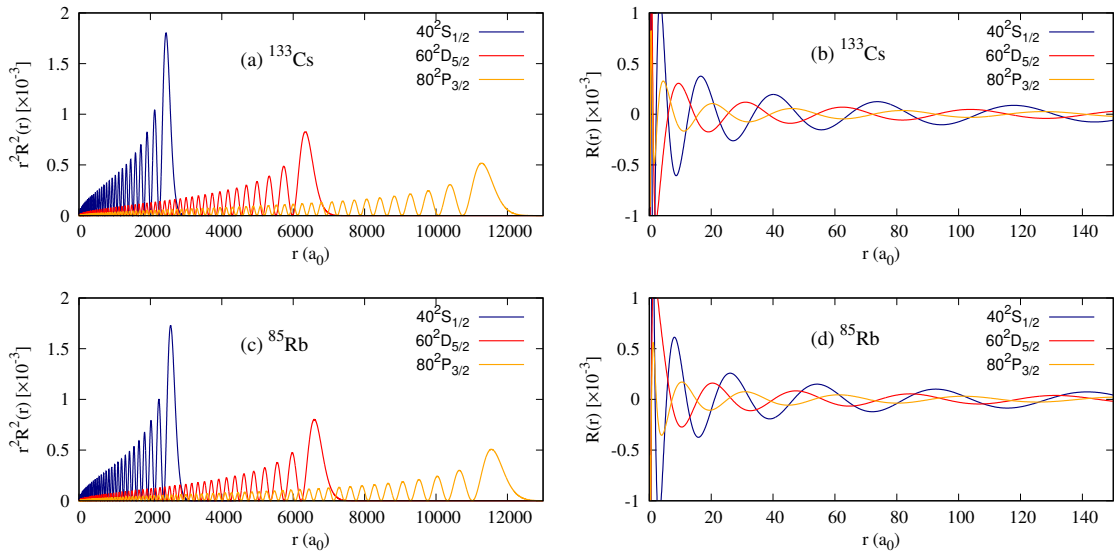

Figure 1.3: Radial probability density function (first column) and radial function (second column) for (a), (b) Cesium and (c), (d) Rubidium atoms in a Rydberg state using the Numerov algorithm [Numerov, 1927].

Inserting the core potential in terms of the variable u, eq. (1.21) then reads

$$\frac{d^2\chi(u)}{du^2} + \left[8\mu Z_{n,l}(u^2) + \frac{4\mu\alpha_c}{u^6}\left(1 - e^{-(u^2/u_c^2)^6}\right) - \frac{4\mu u^2}{(n-\delta_{n,l})^2} - \frac{4l(l+1)+3/4}{u^2}\right]\chi(u) = 0. \tag{1.22}$$

Equation (1.22) is an ordinary differential equation of second-order, which has the form $\chi''(y) + g(y)\chi(y) = 0$ and can be solved using the Numerov algorithm [Numerov, 1927] (see Appendix A). In this algorithm, the continuous solution $y(x)$ is transformed into a discrete solution y_i (evaluated at the i-th step) for integration purposes, and the numerical implementation requires to know *a priori* the values of the function y_0 and y_1 or the values y_N and y_{N-1}, if N is the number of integration steps.

Due to the core potential for alkali-atoms (1.16), the rescaled wavefunction $\chi(u)$ instead of exponentially decay to zero for small values of u, it diverges in this classically forbidden range [Singer, 2004]. Therefore, the range of integration must be truncated, for Rydberg alkali-atoms, the inner radius is set to be $r_a = \alpha_c^{1/3}$, while the outer integration radius is set as $r_b = 2n(n+15)$, which is larger than classical turning point of the wavefunction. In order to minimize the errors at small values u, the integration is performed inwards and we assume that the wavefunction tends to zero at r_b. The error introduced by the range truncation for Rydberg state is only 0.01% [Singer, 2004], setting the radial step of integration as h, then $N = \frac{r_b - r_a}{h}$ and the integration error using the Numerov method scales as $\mathcal{O}(h^6)$.

Up to this point, the Numerov algorithm gives us a radial wavefunction that must be normalized

using a normalization constant $N_{n,l}$, which is found by evaluating the integral

$$N_{n,l} = \int_{r_a}^{r_b} |R'(r)|^2 r^2 dr, \tag{1.23}$$

using cubic interpolation [P. and P., 1967]. The normalized wavefunction $R_{n,l}(r) = R'(r)/\sqrt{N_{nl}}$ allows us to compute matrix elements of the electric multipole operator (see Section 1.1.6) and thus, it is possible to calculate numerically some important properties of Rydberg atoms (see Section 1.2). In order to illustrate the results of the numerical integration, in Tables 1.6 and 1.7, we present the mean radius $\langle r \rangle$ for ^{133}Cs Rydberg atom in a nD state and the radial integrals $\langle n^2 l_j | r | n'^2 l'_{j'} \rangle$ for selected atomic transitions of ^{85}Rb, respectively. Our numerical results compare very well with available experimental data [Lei et al., 1995, O'Sullivan and Stoicheff, 1986], within the experimental error band.

Figure 1.3 shows the radial probability density function $|R_{n,l}|^2 r^2$ and the normalized radial function $R_{n,l}(r)$ for selected Rydberg states of Rubidium and Cesium atoms, in which the Numerov algorithm has been used. The radial density is shifted towards larger radius as the principal quantum number increases, illustrating the large orbital radii of the Rydberg states. The radial function plots still have oscillations near to the core that are flattened as r increases.

1.1.6 Electric multipoles in the fine structure basis

In order to compute the exotic properties of Rydberg atoms, we need to evaluate the matrix elements of the electric multipole using a fine structure basis. The angular part of the matrix elements can be easily calculated using angular momentum algebra, and the radial part can be calculated using the radial wavefunctions obtained following the procedure in Section 1.1.5.

Let us consider the coupled basis $\{|n(ls)jm\rangle\}$ for an atomic state. The matrix elements $I_{ato}(k,q)$ of a spherical tensor operator $\hat{Q}_k^q$ [Zare, 1988], where k is the rank of the operator with components $q = -k, -k+1, ..., k$, are given in the coupled basis by the expression

$$I_{ato}(k,q) = \langle n'(l's')j'm' | \hat{Q}_k^q | n(ls)jm \rangle . \tag{1.24}$$

The dipole moment operator is obtained when $k = 1$ and the quadrupole moment operator when $k = 2$. Equation (1.24) is an atomic integral that can be rewritten using angular momentum algebra and the pure radial wavefuntions showed in the previous section. The spherical tensor operator acts on the electronic coordinates, therefore it does on the orbital angular momentum states which need to be decoupled. From the Wigner-Eckart theorem [Zare, 1988] we have

$$I_{ato}(k,q) = (-1)^{j'-m'} \begin{pmatrix} j' & k & j \\ -m' & q & m \end{pmatrix} \langle n'(l's')j' | |\hat{Q}_k| | n(ls)j \rangle . \tag{1.25}$$

where the circular brakets are the $3j$-symbols and $\langle n'(l's')j' | |\hat{Q}_k| | n(ls)j \rangle$ is the reduced matrix element [Zare, 1988]. Using angular momentum algebra the reduced matrix element can be de-

coupled as [Zare, 1988]

$$\langle n'(l's')j'|\,|\hat{Q}_k|\,|n(ls)j\rangle = \delta_{s's}(-1)^{j+l'+s'+k}[j']^{1/2}[j]^{1/2}\begin{Bmatrix} l' & j' & s \\ j & l & k \end{Bmatrix}\langle n'l'|\,|\hat{Q}_k|\,|nl\rangle\,, \quad (1.26)$$

where $[j] \equiv 2j+1$. The curly brakets is a $6j$-symbol [Zare, 1988] and the integral $\langle n'l'|\,|\hat{Q}_k|\,|nl\rangle$ is the orbital reduced matrix element. These matrix elements can be evaluated using the angular momentum wavefunctions Y_l^m and the Wigner-Eckart theorem, which are given by

$$\langle n'l'|\,|\hat{Q}_k|\,|nl\rangle = (-1)^{l'}[l']^{1/2}[l]^{1/2}\begin{pmatrix} l' & k & l \\ 0 & 0 & 0 \end{pmatrix}\langle n'l'|\,\hat{Q}_k\,|nl\rangle\,. \quad (1.27)$$

The radial atomic integrals $\langle n'l'|\,\hat{Q}_k\,|nl\rangle$ can be computed by solving the electronic structure according to the previous section and represent the overlap of the wavefunctions and the tensor operator,

$$\langle n'l'|\,\hat{Q}_k\,|nl\rangle = \int_{r_i}^{r_f} R_{n'l'}(r)\hat{Q}_k(r)R_{nl}(r)r^2dr. \quad (1.28)$$

Finally, using eqs. (1.27), (1.26) and (1.25), we obtain the final expression

$$\begin{aligned} I_{ato}(k,q) &= \delta_{s's}(-1)^{j'+j-m+s+k}[l']^{1/2}[l]^{1/2}[j']^{1/2}[j]^{1/2}\begin{pmatrix} l' & k & l \\ 0 & 0 & 0 \end{pmatrix} \\ &\times \begin{pmatrix} j' & k & j \\ -m' & q & m \end{pmatrix}\begin{Bmatrix} l' & j' & s \\ j & l & k \end{Bmatrix}\langle n'l'|\,\hat{Q}_k\,|nl\rangle\,. \end{aligned} \quad (1.29)$$

1.2 Atomic polarizability function

In this section, we discuss the dynamical polarizability function of Rydberg atoms using the results from previus sections. This function is relevant to study the long-range interaction between Rydberg atoms and molecules in the next chapters.

We start by considering the general expression of the qq-component of the dynamical polarizability function shown in Appendix B (eq. (B.23), for an atomic state $k = |n(ls)jm\rangle$

$$\begin{aligned} \alpha_{qq'}^{nljm}(\omega) &= 2(-1)^q \sum_{n'}\sum_{l's'}\sum_{j'm'}\frac{(E_{n'l'j'} - E_{nlj})}{(E_{n'l'j'} - E_{nlj})^2 - \omega^2} \\ &\langle n(ls)jm|\hat{Q}_1^q|n'(l's')j'm'\rangle\,\langle n'(l's')j'm'|\hat{Q}_1^{-q'}|n(ls)jm\rangle\,, \end{aligned} \quad (1.30)$$

where $\hat{Q}_1^q$ is the dipole moment operator. Expression (1.30) can be further developed for angular momentum states. Since the dipole operator ($\hat{Q}_1^q$) acts over the electronic angular momentum state $|lm_l\rangle$, the matrix elements $\langle nljm|\hat{Q}_1^{-q}|n'(l')j'm'\rangle$ can be rewritten using eq. (1.29). From the symmetry properties of $3j$-symbols [Zare, 1988], the only non-zero components of the polarizabil-

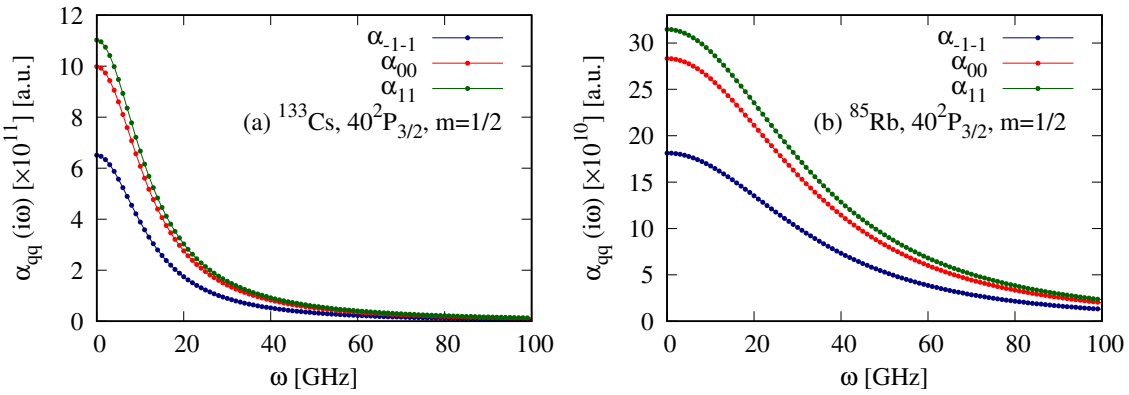

Figure 1.4: Atomic dynamical polarizability function components calculated for Rydberg states $40^2P_{3/2},\ m = 1/2$ of (a)^{133}Cs and (b)^{85}Rb at imaginary frequency $\alpha_{qq}(i\omega)$.

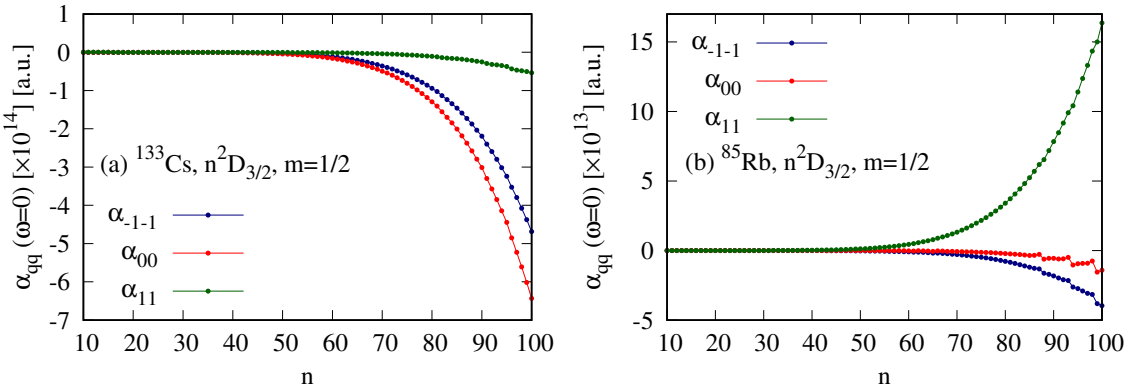

Figure 1.5: Atomic static polarizability components $\alpha_{qq}(\omega = 0)$ calculated for $n^2D_{3/2},\ m = 1/2$ Rydberg states of ^{133}Cs and ^{85}Rb atoms.

ity are those for which $q = q'$, thus α_{qq}^{nljm} is given by

$$\alpha_{qq}^{nljm}(\omega) = \delta_{ss'} \sum_{n'l'j'm'} (-1)^{2j'+2j-m'-m+q+1} \left[\frac{2(E_{n'l'j'} - E_{nlj})}{(E_{n'l'j'} - E_{nlj})^2 - \omega^2} [j][l][j'][l'] \right.$$
$$\left. \times \begin{pmatrix} l' & 1 & l \\ 0 & 0 & 0 \end{pmatrix}^2 \begin{Bmatrix} l & j & s \\ j' & l' & 1 \end{Bmatrix}^2 \begin{pmatrix} j' & 1 & j \\ -m' & -q & m \end{pmatrix}^2 |\langle n'l'|er|nl\rangle|^2 \right]. \quad (1.31)$$

We use eq. (1.31) to compute the non-zero components of the polarizability for Rydberg atomic states ($n \geq 15$) and include all intermediate states in the summation (1.31) to ensure its convergence, that is $n' = n \pm 10$, giving a relative change $\delta\alpha/\alpha$ smaller than a fixed tolerance $\varepsilon = 0.01$.

Figure 1.4 shows the atomic dynamical polarizability components α_{qq}^{nljm} evaluated at imaginary frequency for ^{133}Cs and ^{85}Rb in a $40^2P_{3/2},\ m = 1/2$ Rydberg state. The polarizability function tends quickly to zero. Figure 1.5 shows how the static values of the polarizability increases in magnitude as a functions of the principal quantum number n for ^{133}Cs and ^{85}Rb in a $n^2D_{3/2},\ m = 1/2$.

n	α_{sca}(theo)	α_{sca}(exp)	%error	|error|	α_{ten}(theo)	α_{ten}(exp)	%error	|error|	α_{00}^{nljm}(theo)
15	8.42[7]	8.60[7]	2.34	0.20[7]	3.72[7]	3.54[7]	5.23	0.19[7]	4.70[7]
20	6.25[8]	6.43[8]	2.50	0.16[8]	3.62[8]	3.58[8]	1.35	0.05[8]	2.63[8]
25	2.76[9]	2.97[9]	7.00	0.19[9]	2.08[9]	2.01[9]	3.40	0.07[9]	0.68[9]
30	1.05[10]	1.05[10]	0.40	0.042[9]	7, 80[9]	7.84[9]	0.51	0.04[9]	2.70[9]
35	2.69[10]	2.97[10]	5.40	0.15[10]	2.57[10]	2.49[10]	3.39	0.087[10]	0.12[10]
40	7.45[10]	7.43[10]	0.27	0.02[10]	6.61[10]	6.43[10]	3.13	0.20[10]	0.84[10]
45	1.60[11]	1.69[11]	4.80	0.077[11]	1.59[11]	1.57[11]	1.03	0.01[11]	0.01[11]
50	3.43[11]	3.42[11]	0.50	0.017[11]	3.35[11]	3.30[11]	1.83	0.06[11]	0.08[11]
55	5.95[11]	6.59[11]	9.80	0.58[11]	6.99[11]	6.55[11]	6.75	0.47[11]	-1.04[11]

Table 1.8: Scalar and tensor static polarizabilities for ^{85}Rb in $n^2D_{3/2}$ state calculated theoretically in this work (theo) and compared with the experimental data available [O'Sullivan and Stoicheff, 1986] (exp). The %error and the corresponding absolut value of error for each polarizability component are also shown. The last column shows the 00-component of the polarizability $\alpha_{00}^{nljm} = \alpha_{sca}$ - α_{teo} for $j = 3/2,\ m = 1/2$. The square parenthesis $A[x]$ in the fifth column means $A \times 10^x$.

Error estimation

Figures 1.6 and 1.7 show the 00-component of the static polarizability as a function of the principal quantum number n in different angular momentum states $|n^2l_j\rangle$ compared with the available experimental data for ^{133}Cs and ^{85}Rb. Most of the results obtained are in good agreement with the data, except for Rubidium in $D_{3/2},\ m = 1/2$ state. Due to the non-monotonic behavior of this polarizability in the range of n between 30 and 60 (see Fig. 1.7(c)), we consider it as a separate case.

The 00-component of the atomic polarizability (1.31) can also be written in tensorial form, which allows to define a scalar and tensor polarizability as follows [Bonin and Kresin, 1997]

$$\alpha_{00}^{nljm} = \alpha_{sca}(j) + \alpha_{ten}(j)\frac{3m^2 - j(j+1)}{j(2j-1)}. \tag{1.32}$$

For the state $n^2D_{3/2},\ m = 1/2$, we compute and compare the scalar (α_{sca}) and tensor (α_{ten}) static polarizabilities using the sum-over-states expressions given in eq. (1.32). The results are shown in Table 1.8. The 00-component of the polarizability in terms of α_{sca} and α_{ten} is given by $\alpha_{00}^{nljm} = \alpha_{sca} - \alpha_{ten}$ for $j = 3/2$ and $m = 1/2$. For $n = 35, 45$, we found that the static polarizability α_{00}^{nljm} (see last column of Table 1.8) is smaller than the error values of its corresponding scalar and tensor components. For states with $n = 25, 40, 50$ the total polarizability is of the order of the error. We conclude that in the region $30 < n < 60$, the error band does not allow us to estimate a reliable polarizability for Rubidium $^2D_{3/2},\ m = 1/2$ states.

For the rest of the atomic states of Rubidium and for all the atomic states of Cesium the estimated errors for the qq-components of the polarizabilities are less than 1% compared with the available experimental data.

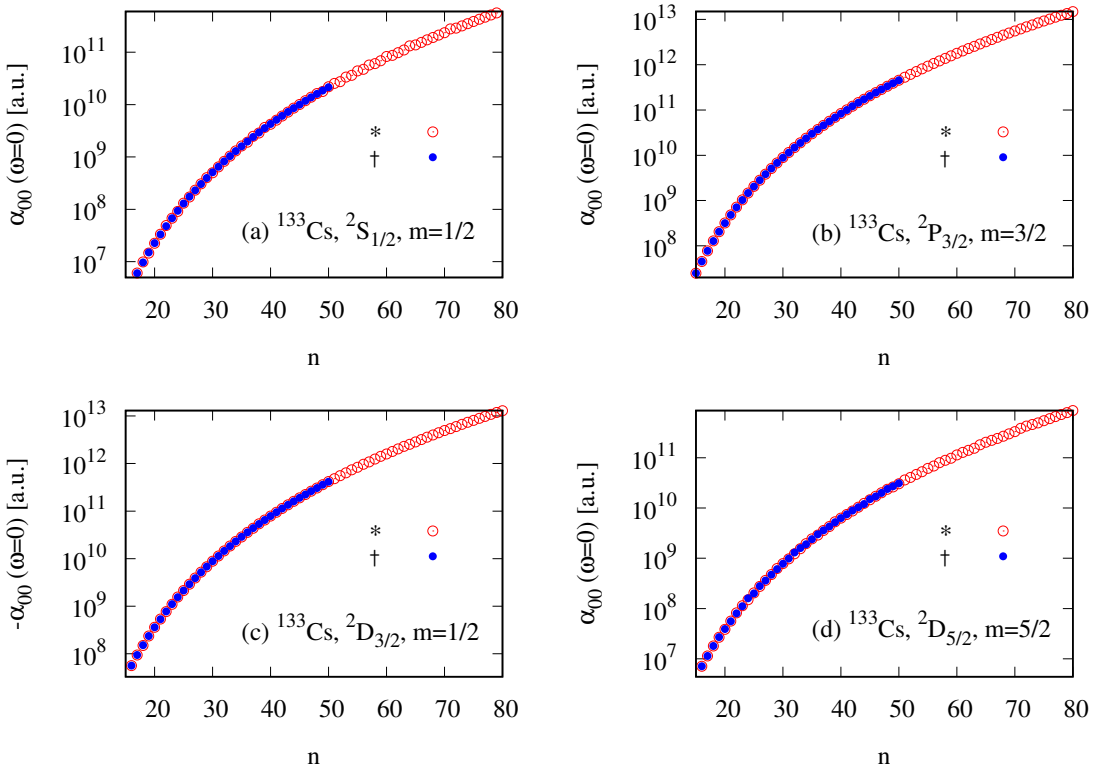

Figure 1.6: 00-component of the atomic static polarizability $\alpha_{00}(\omega = 0)$ computed for several Rydberg states of ^{133}Cs and compared with the avalaible data. This work*, [Yerokhin et al., 2016]†.

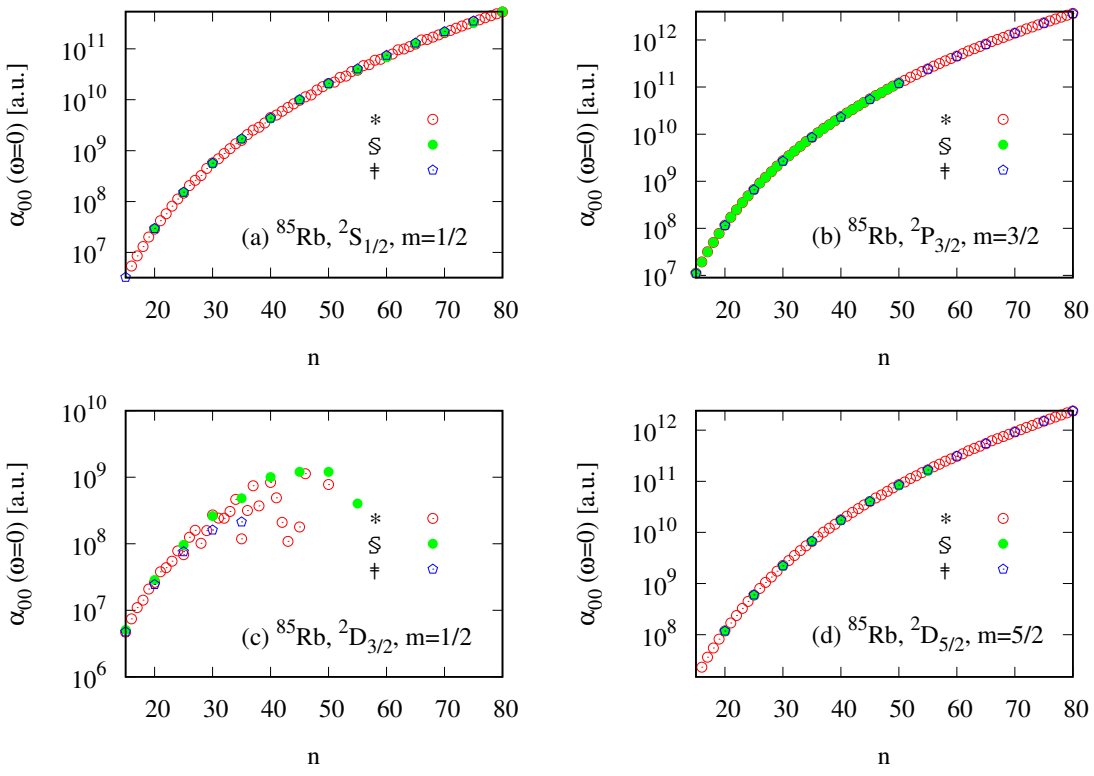

Figure 1.7: 00-component of the atomic static polarizability $\alpha_{00}(\omega = 0)$ computed for several Rydberg states of ^{85}Rb and compared with the avalaible data. This work*, [O'Sullivan and Stoicheff, 1986]§, [Lai et al., 2018]‡. For $^2D_{3/2}$ $m = 1/2$ state, there are visible dicrepancies between all references, this is explained using eq. (1.32) and Table 1.8.

Chapter 2

Heteronuclear Diatomic Molecules

The complete mechanical description of the simplest diatomic molecule is difficult to achieve, even classically. In 1927, Born and Oppenheimer [Born and Oppenheimer, 1927] established a good approximation to describe an isolated molecule, in which the molecule is characterized by its several types of motion, namely, translational, rotational, vibrational and electronic. This approximation relies on by the difference between the masses of the electrons and the nuclei that form the molecule. The electron mass m is about four orders of magnitude smaller than the mass of the nucleus M. Therefore, electrons can move much faster than nuclei. Born and Oppenheimer proposed the separation of the electronic and nuclear motion in the molecule by setting the parameter

$$\kappa = \left(\frac{m}{M}\right)^{1/4} \sim \frac{1}{10}, \tag{2.1}$$

and showed that

$$\frac{\Delta E_{nuc}}{\Delta E_{ele}} \approx \kappa^2, \qquad \frac{\Delta E_{rot}}{\Delta E_{vib}} \approx \kappa^2, \tag{2.2}$$

where ΔE_{nuc}, ΔE_{ele}, ΔE_{rot} and ΔE_{vib} are the separation between nuclear, electronic, rotational and vibrational energy levels, respectively. This energy classification is well-known as the *Born–Oppenheimer separation* and is very appropriate for molecules in closed shell ground states.

This Chapter discusses the fundamentals of closed shell diatomic molecules using the Born-Oppenheimer approximation. In order to find the molecular wavefuntion, the Born adiabatic approximation and the rigid rotor model are also used. The molecular eigenstates and eigenvalues are used to compute the molecular dynamical polarizability, which will be needed to study the long-range interaction between Rydberg atoms and ground state molecules.

2.1 Molecular Hamiltonian and wavefunctions

The internal kinetic energy of a diatomic molecule can be written in terms of kinetic energy operator of the eletrons and nuclei in the laboratory frame as [Brown and Carrington, 2003] (atomic units)

$$T = -\sum_{\beta=1}^{2} \frac{\nabla_\beta^2}{2M_\beta} - \sum_{i=1}^{N_e} \frac{\nabla_i^2}{2}, \tag{2.3}$$

where β and i are sums over the nuclei of masses M_β and the N_e electrons, respectively. We transform the kinetic energy expression (2.3) in the space-fixed frame to the center of mass of the nuclei, located at

$$\mathbf{R}_N = \frac{\sum_\beta M_\beta \mathbf{R}_\beta}{M_1 + M_2}. \tag{2.4}$$

Using the internuclear vector $\mathbf{R} = \mathbf{R}_2 - \mathbf{R}_1$, the kinetic energy defined in a system frame where the origin is at center of the nuclei is given by [Brown and Carrington, 2003]

$$T = -\frac{\nabla_N^2}{2M_N} - \frac{\nabla_R^2}{2\mu_{mol}} - \sum_i \frac{\nabla_i^2}{2} - \sum_{ij} \frac{\nabla_i \nabla_j'}{2M_N}, \tag{2.5}$$

where $M_N = M_1 + M_2$ is the total mass of the nuclei and their reduced mass is defined as $\mu_{mol} = M_1 M_2 / M_N$. The first term on the right-hand side of eq. (2.5) represents the kinetic energy due to the translational motion of the molecule, which can be ignored in the absence of spacially inhomogeneous external fields. The second term is the kinetic energy of the nuclei, which describes the vibrational and rotational motion. The term $-\sum_i \frac{\nabla_i'^2}{2}$ is the kinetic energy of the electrons. The last term $-\sum_{ij} \frac{\nabla_i' \nabla_j'}{2M_N}$ is commonly known as the mass polarisation term and accounts for the small fluctuations of the position of the center of mass of the nuclei due to the movement of the electrons within the molecule.

The non-relativistic molecular Hamiltonian $\mathcal{H}_{mol}$ of a diatomic molecule in free space can thus be separated into electronic and nuclear contributions

$$\mathcal{H}_{ele} = -\frac{1}{2}\sum_i \nabla_i^2 - \frac{1}{2M_N}\sum_{i,j} \nabla_i \cdot \nabla_j + \sum_{i \neq j} \frac{1}{R_{ij}} - \sum_{i,\beta} \frac{Z_\beta}{R_{i\beta}}, \tag{2.6}$$

$$\mathcal{H}_{nuc} = -\frac{1}{2\mu_{mol}} \nabla_R^2 + \frac{Z_1 Z_2}{R}. \tag{2.7}$$

These Hamiltonians contain the kinetic energy terms from eq. (2.5) and the potential energy correponding to the interaction between the particles. Z_β is the atomic charge of the nucleus and $R_{a,b}$ is the relative distance between the particle $a = i, j$(electrons) and $b = j$(electron), β(nucleus).

The Schrödinger equation of a diatomic molecule in a field-free space is thus written in the molecule-fixed frame as

$$(\mathcal{H}_{ele} + \mathcal{H}_{nuc})\Psi_{rve} = E_{rve}\Psi_{rve}, \tag{2.8}$$

where $\Psi_{rve} = \Psi_{rve}(\mathbf{r}_i, R, \theta, \varphi)$ is the total molecular wavefunction which depends on the electronic coordinates $\mathbf{r}_i$ and the nuclear spherical coordinates (R, θ, φ). Since the electron mass is

approximately 1800 times smaller than the nuclear mass, the ratio m_e/μ_{mol} is very small, and the nuclear Hamiltonian $-\frac{1}{2\mu_{mol}}\nabla^2_R$ is a perturbing operator compared with the electronic Hamiltonian [Herrera, 2012]. Therefore, The zero-th order wavefunctions are written as the product of electronic and nuclear states as $\Psi^{(0)}_{rve} = \Psi^{(0)}_e \Psi^{(0)}_{rv}$. This is known as the Born–Oppenheimer approximation.

The molecular wavefunction Ψ_{rve} can be expanded as complete set of orthonormal electronic Ψ^n_e and nuclear Ψ^n_{rv} functions as

$$\Psi_{rve} = \sum_n a_n \Psi^n_e(\mathbf{r}_i, R)\Psi^n_{rv}(R, \theta, \varphi). \tag{2.9}$$

The eigensystem for the electronic Hamiltonian is written as

$$\mathcal{H}_{ele}\Psi^n_e(\mathbf{r}_i, R) = E^n_e \Psi^n_e(\mathbf{r}_i, R) \tag{2.10}$$

where $\int d\mathbf{r}^3_i[\Psi *^{n'}_e \Psi^n_e] = \delta_{nn'}$. Each fixed distance R determines different configurations of the electronic coordinates $\mathbf{r}_i$ to solve eq. (2.10), making the electronic equation to depend parametrically depend on the internuclear distance.

Replacing eq. (2.9) into (2.8), multiplying from the left by $\Psi^{*n'}_e$ and integrating over the electronic coordinates to give

$$a_n \left(E^n_e + V_{nuc} - E_{rve}\right)\Psi^n_{rv} + \sum_n a_n C_{n'n}\Psi^n_{rv} = 0, \tag{2.11}$$

where $V_{nuc} = \frac{Z_1 Z_2}{R}$ and $C_{n'n}\Psi^n_{rv} = \int \Psi^{*n'}_e \left(-\frac{1}{2\mu_{mol}}\nabla^2_R\right)\Psi^n_e d\mathbf{r}_i \Psi^n_{rv}$ are the non-adiabatic coupling functions. The nuclei are assumed to be fixed in space, and electrons follow the nuclear motion adiabatically, i.e. the electronic state is changing very slowly according to the nuclear displacements, i.e. $C_{nn'}\Psi^n_{rv} \approx \left(-\frac{1}{2\mu_{mol}}\nabla^2_R\right)\delta_{nn'}\Psi^n_{rv}$, and the nuclear Schrödinger equation (2.11) becomes

$$\left[-\frac{1}{2\mu_{mol}}\nabla^2_R + V_{nuc} + E^n_e\right]\Psi^n_{rv}(R, \theta, \varphi) = \mathcal{E}_{rve}[\Psi^n_{rv}(R, \theta, \varphi)]. \tag{2.12}$$

Following the procedure in Chapter 1, Section 1.1.1 we can write the operator ∇^2_R as

$$\nabla^2_R = \frac{1}{R^2}\frac{\partial}{\partial R}\left(R^2\frac{\partial}{\partial R}\right) + \frac{\csc\theta}{R^2}\frac{\partial}{\partial\theta}\left(\sin\theta\frac{\partial}{\partial\theta}\right) + \frac{\csc^2\theta}{R^2}\left(\frac{\partial^2}{\partial\varphi^2}\right) \tag{2.13}$$

The first term is related to the vibrational motion of the nuclei and the rest is of the expression related to the rotational motion. By introducing the angular momentum operator $\mathbf{J}$ of the molecular system as

$$\mathbf{J}^2 = \csc\theta\frac{\partial}{\partial\theta}\left(\sin\theta\frac{\partial}{\partial\theta}\right) + \csc^2\theta\frac{\partial^2}{\partial\varphi^2}, \tag{2.14}$$

we simplify the expression for the operator (2.13) to read

$$\nabla^2_R = \frac{1}{R^2}\frac{\partial}{\partial R}\left(R^2\frac{\partial}{\partial R}\right) + \frac{\mathbf{J}^2}{R^2}. \tag{2.15}$$

The nuclear wavefunction can be solved by separating the radial and the angular dependence

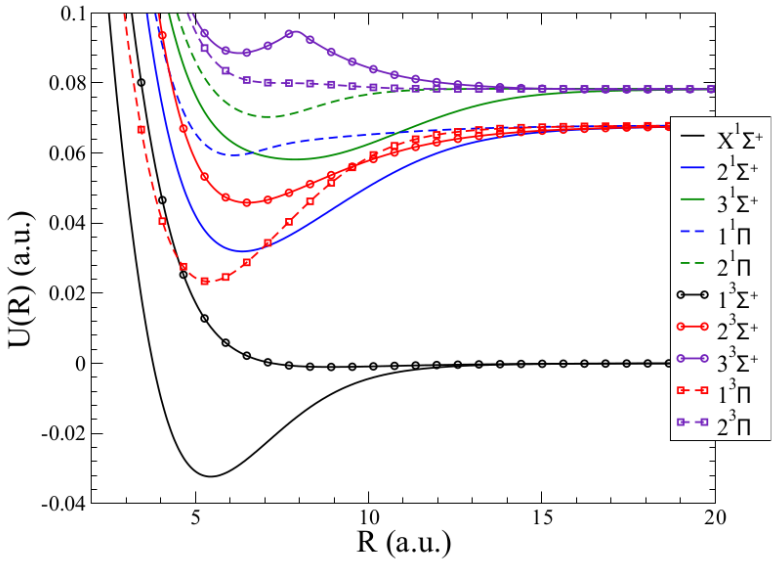

Figure 2.1: Lowest ten electronic potentials of the ^{23}Na^{6}Li molecule. The energy $U(r)$ is in atomic units (a.u.) and R in units of Bohr radius a_0. Potentials are taken from Ref. [Wang, 2014].

(vibrations and rotations) as

$$\phi^n_{rv}(R,\theta,\varphi) = \frac{S(R)}{R} Y^M_J(\theta,\varphi), \tag{2.16}$$

where $Y^M_J(\theta,\varphi)$ are spherical harmonics with M being the component of total angular momentum $\mathbf{J}$ along the space-fixed z-axis. The spherical harmonics functions obey the relation

$$\mathbf{J}^2 Y^M_J = J(J+1) Y^M_J, \tag{2.17}$$

and they correspond to angular momentum states of the system, i.e.

$$|JM\rangle = Y^M_J(\theta,\varphi). \tag{2.18}$$

Applying the angular momentum state relation (2.17) into eq. (2.12), we obtain a radial nuclear equation of the form

$$\left[-\frac{1}{2\mu_{mol}}\left(\frac{d^2}{dR^2}\right) + \frac{J(J+1)}{2\mu_{mol}R^2} + V(R)\right] S(R) = \mathcal{E}_{rve} S(R). \tag{2.19}$$

The second term is the rotational energy that acts as a centrifugal barrier to the vibrational motion. The effective nuclear potential is $V(R) = V_{nuc}(R) + E^n_e(R)$.

The radial wavefuntion describes the vibration of the nuclei about a given position (R) and the angular wavefunction describes the rotation of the molecule about its center of mass. In general, even when this separation of varibles has been done, these two types of motions are coupled [Brown and Carrington, 2003].

To solve eq. (2.19), it is necessary to know $V(R)$, which is found by solving the electronic Schrödinger equation (2.10) for several internuclear distances, giving potential curves for $V(R)$

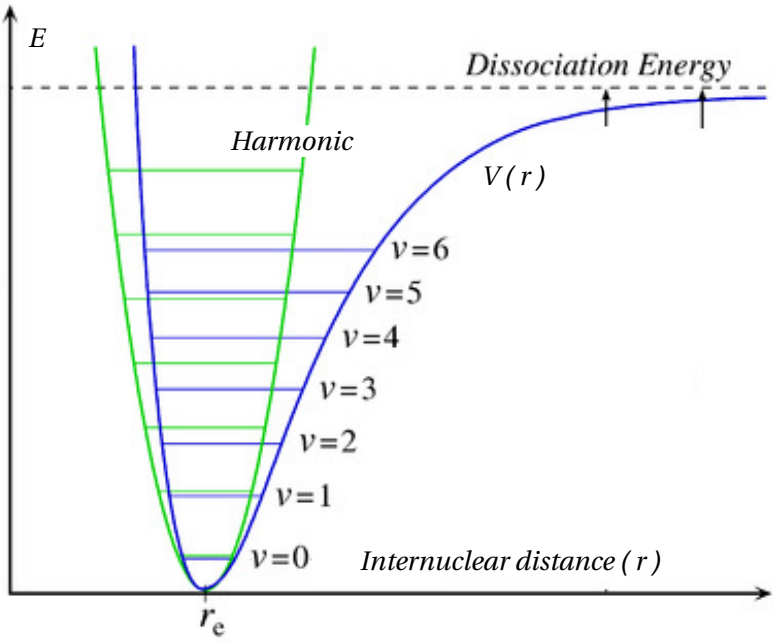

Figure 2.2: Molecular electronic potential displaying several vibrational levels and comparison with the harmonic approximation around the equilibrium position R_e.

like those shown in Figure 2.1 for ^{23}Na^{6}Li molecules.

Figure 2.2 shows a typical electronic potential curve. For $R \to 0$ the potential represents a strong repulsive barrier between the nuclei. As R increases, the potential energy reaches its minimum value at equilibrium position R_e. From this point the potential increases with R, tending to an asymptotic value at $R \to \infty$, where molecules eventually dissociate.

Back to the radial equation (2.19), $V(R)$ can be expressed as a Taylor series around the equilibrium position (R_e) obtaining

$$V(R) = \frac{k_e}{2}(R - R_e)^2, \qquad k_e = \frac{d^2V(R_e)}{dR^2}. \tag{2.20}$$

This is an harmonic potential model and it works for low rotational levels (near the equilibrium position R_e). Replacing (2.20) into (2.19) and taking $R = R_e$ for the rotational energy, the radial equation (2.19) becomes

$$\left[-\frac{1}{2\mu_{mol}}\left(\frac{d^2}{dR^2}\right) + \frac{J(J+1)}{2\mu_{mol}R_e^2} + \frac{k_e}{2}(R - R_e)^2\right] S(R) = \mathcal{E}_{rve}S(R). \tag{2.21}$$

Setting $R = R_e$ to obtain eq. (2.21) is known as the *rigid rotor* approximation, which states that while the molecule rotates the internuclear distance does not change. The mathematical justification is supported by a Taylor series of a rotational term about R_e.

Finally, with $q = R - R_e$ and the rotational term $\frac{J(J+1)}{2\mu_{mol}R_e^2} = E_{rot}$, eq. (2.21) is rewritten as

$$\left[-\frac{1}{2\mu_{mol}}\left(\frac{d^2}{dq^2}\right) + \frac{k_e}{2}q^2\right] S(q) = (\mathcal{E}_{rve} - E_{rot})\, S(R). \tag{2.22}$$

The energy levels for this harmonic oscillator are given by[1]

$$E_{vib} = \left(v + \frac{1}{2}\right) h\nu_e, \qquad \nu_e = \frac{1}{2\pi}\left(\frac{k_e}{\mu_{mol}}\right)^{\frac{1}{2}}, \qquad v = 0, 1, 2, 3, ... \tag{2.23}$$

The rovibrational energies of diatomic molecules in the rigid rotor approximation are thus given by

$$E_{vJ} = \left(v + \frac{1}{2}\right) hv_e + J(J+1)B_e. \tag{2.24}$$

Where $B_e = \frac{1}{2\mu_{mol}R_e}$ (in atomic units) is the *rotational constant*, which ranges between 1-20 GHz for alkali-heteronuclear diatomic molecules [Deiglmayr et al., 2008a].

The rigid rotor and harmonic oscillator models are approximations valid for low excited energy levels (vibrational and rotational). For higher excited levels, it is required to take more terms in the Taylor series for the potential $V(q)$, in a general form [Brown and Carrington, 2003]

$$V(q) = a_0 q^2 (1 + a_1 q + a_2 q^2 + a_3 q^3 + ...), \tag{2.25}$$

where $a_0 = hw_e^2/4B_e$ and a_i with $i = 1, 2, 3...$ are constants. Equation (2.25) represents the anharmonic deviations of the harmonic model (2.20). The rotational term can also be expanded as a power series in q as (Planck constant $h = 1$)

$$H_{rot} = \frac{1}{2\mu_{mol}R_e} J(J+1)[1 + c_1 q + c_2 q^2 + c_3 q^3 + ...], \tag{2.26}$$

where c_i with $i = 1, 2, 3...$ are constants. Equations (2.25) and (2.26) can be treated using ordinary non-degenerate perturbation theory [Brown and Carrington, 2003], giving a total rovibrational energy of the form

$$E_{(v,J)} = \sum_{kl} Y_{kl} (v + 1/2)^k J^l (J+1)^l. \tag{2.27}$$

The coefficients Y_{kl} are explicitly given by Dunham [Dunham, 1932]. Equation (2.27) is well-known as the Dunham expansion.

In general, the vibrational energy is about three orders of magnitude greater than the rotational energy $v_e > B_e$. This is due to the dependence with the reduced mass; $v_e \propto \mu_{mol}^{-\frac{1}{2}}$, while $B_e \propto \mu_{mol}^{-1}$. Therefore, a mainfold of rotational energy levels are associated to one particular vibrational state [Carr et al., 2009]. There is another relevant energy scale, corresponding to the changes in the electronic levels. This energy scale is at least two orders of magnitude greater than the vibrational energy [Carr et al., 2009].

So far we have not considered the interaction Hamiltonian of the electronic angular momentum and the electronic spin $\mathcal{H}(\mathbf{L}, \mathbf{S})$, which is related to smaller energy scales in the molecular structure. Considering this interaction Hamiltonian, the general form of the angular momentum states

[1] Using the harmonic oscillator model it is found that $S_v(q) = (\frac{\alpha}{\Pi})^{1/4} \frac{\mathbf{H}_v(\alpha^{1/2}q) \exp -\alpha q^2/2}{(2^v v!)^{1/2}}$ [Schwabl, 2007]. $\mathbf{H}_v$ are the Hermite polynomials, $\alpha = \frac{\mu_{mol}\omega_e}{\hbar}$ and $\omega_e = 2\pi v_e$.

becomes [Brown and Carrington, 2003]

$$|J\Omega M\rangle = \left[\frac{2J+1}{4\pi}\right]^{1/2} \mathcal{D}^{(J)}_{M\Omega}(\theta,\varphi,\chi), \tag{2.28}$$

and the rotational energy is given by

$$E_{rot} = \frac{1}{2\mu_{mol}R^2}\left[J(J+1) - \Omega^2\right] \tag{2.29}$$

where $\Omega = \Lambda + \Sigma$, which are the eigenvalues of the operators $\mathbf{L}_z$ and $\mathbf{S}_z$, respectively, and $\mathcal{D}^{(J)}_{M\Omega}$ is an element of the Wigner rotation matrix [Zare, 1988] specified by the Euler angles (θ,φ,χ) [Zare, 1988].

Since we work with closed-shell molecules in the $X^1\Sigma^+$ state, all the electronic angular momenta are zero ($\mathbf{L} = \mathbf{S} = \mathbf{0}$), therefore $\Omega = 0$ and eq. (2.28) becomes

$$|J0M\rangle = \left[\frac{2J+1}{4\pi}\right]^{1/2} \mathcal{D}^{(J)}_{M0}(\theta,\varphi) = Y^M_J, \tag{2.30}$$

as given in eq. (2.16).

Finally, the state for an isolated diatomic molecule under the Born–Oppenheimer approximation and the rigid rotor model is thus written as

$$\Psi_{rve} \equiv |\gamma\rangle\,|vJ\rangle\,|J\Omega M\rangle\,, \tag{2.31}$$

where $|\gamma\rangle$ denotes de electronic state, $|vJ\rangle$ is the rovibrational state and $|J\Omega M\rangle$ is angular momentum state. For molecules in the electronic and rovibrational ground state, in which we are interested, the system state is given by $|X^1\Sigma^+\rangle\,|v=0,J=0\rangle\,|J=0,\Omega=0,M=0\rangle$.

2.2 Molecular polarizability function

In this section, we study the frequency-dependent polarizability of ground state molecules ($X^1\Sigma^+, v = 0, J = 0$) and compute this function for KRb, LiCs, LiRb and RbCs molecules. We focus on the low-frequency regime, in which these molecules interact at long-range distances with Rydberg alkali-atoms.

In the space-fixed frame, the dynamical dipole polarizability components (see Appendix B) for a molecular state $|\gamma vJ\Omega M\rangle$ with energy $E_{\gamma vJ}$ can be written as

$$\begin{aligned}\alpha^{\gamma vJ\Omega M}_{qq'}(\omega) \;=\; & \sum_{\gamma'v'}\sum_{J'\Omega'M'}\Bigg[\frac{2(-1)^q(E_{\gamma'v'J'} - E_{\gamma vJ})}{(E_{\gamma'v'J'} - E_{\gamma vJ})^2 - \omega^2} \times \\ & \langle\gamma vJ\Omega M|\hat{Q}^q_1|\gamma'v'J'\Omega'M'\rangle\,\langle\gamma'v'J'\Omega'M'|\hat{Q}^{-q'}_1|\gamma vJ\Omega M\rangle\Bigg].\end{aligned} \tag{2.32}$$

Where $\hat{Q}_1^q$ is a multipole moment, a spherical tensor operator of rank 1 and component q. To evaluate the molecular dipole integrals $\langle \gamma v J\Omega M|\hat{Q}_1^q|\gamma' v' J'\Omega' M'\rangle$ in the space-fixed frame, the q-component of the dipole operator must be written in terms of the molecule-fixed p-components through the unitary transformation $\hat{Q}_1^q = \sum_p \mathcal{D}_{qp}^{*(1)}\hat{Q}_1^p$. Transforming to the molecule-fixed frame is convenient since the electronic and nuclear eigenfunctions are usually computed in the molecule-fixed frame. The matrix elements of the spherical tensor operator are given by

$$\langle \gamma v J\Omega M|\hat{Q}_1^q|\gamma' v' J'\Omega' M'\rangle = \sum_p \langle J\Omega M|\mathcal{D}_{qp}^{*(1)}|J'\Omega' M'\rangle \langle \gamma v|\hat{Q}_1^p|\gamma' v'\rangle . \tag{2.33}$$

The matrix elements $\langle J\Omega M|\mathcal{D}_{qp}^{*(1)}|J'\Omega' M'\rangle$ can be evaluated using the expression for the angular integral of the Wigner rotation matrix [Zare, 1988]

$$\int \mathcal{D}^{J_3}_{M_3' M_3}(K)\mathcal{D}^{J_2}_{M_2' M_2}(K)\mathcal{D}^{J_1}_{M_1' M_1}(K)dK = 8\pi^2 \begin{pmatrix} J_1 & J_2 & J_3 \\ M_1' & M_2' & M_3' \end{pmatrix} \begin{pmatrix} J_1 & J_2 & J_3 \\ M_1 & M_2 & M_3 \end{pmatrix}, \tag{2.34}$$

where $dK = d\varphi \sin\theta d\theta d\chi$ is the solid angle element and the circular brakets are the $3j$-symbols [Zare, 1988]. Therefore, the matrix element $\langle J\Omega M|\mathcal{D}_{qp}^{*(1)}|J'\Omega' M'\rangle$ can be written as

$$\langle J\Omega M|\mathcal{D}_{qp}^{*(1)}|J'\Omega' M'\rangle = (-1)^{M-\Omega}\sqrt{(2J+1)(2J'+1)} \begin{pmatrix} J' & 1 & J \\ -M' & -q & M \end{pmatrix} \begin{pmatrix} J' & 1 & J \\ -\Omega' & -p & \Omega \end{pmatrix}, \tag{2.35}$$

and eq. (2.32) becomes

$$\begin{aligned} \alpha_{qq'}^{\gamma v J\Omega M}(\omega) = \sum_{\gamma', v'} \sum_{J'\Omega' M'} & 2(-1)^{M+M'-\Omega-\Omega'} \frac{E_{\gamma' v' J'} - E_{\gamma v J}}{(E_{\gamma' v' J'} - E_{\gamma v J})^2 - (\omega)^2} \\ & \times [J][J'] \begin{pmatrix} J' & 1 & J \\ -M' & -q & M \end{pmatrix} \begin{pmatrix} J' & 1 & J \\ -M' & q' & M \end{pmatrix} \\ \times \sum_{pp'} & \begin{pmatrix} J' & 1 & J \\ -\Omega' & -p & \Omega \end{pmatrix} \begin{pmatrix} J & 1 & J' \\ -\Omega & -p' & \Omega' \end{pmatrix} \langle \gamma v|\hat{Q}_1^p|\gamma' v'\rangle \langle \gamma' v'|\hat{Q}_1^{p'}|\gamma v\rangle , \end{aligned} \tag{2.36}$$

where $[J] \equiv 2J+1$. According to the symmetry properties of the $3j$-symbols [Zare, 1988], the non-vanishing terms in eq. (2.36) are those with $q' = q$ and $-p = p'$. Expression (2.36) is then rewritten as

$$\begin{aligned} \alpha_{qq}^{\gamma v J\Omega M}(\omega) = \sum_{\gamma', v'} \sum_{J'\Omega' M'} & 2(-1)^{M+M'-\Omega-\Omega'}[J][J'] \frac{E_{\gamma' v' J'} - E_{\gamma v J}}{(E_{\gamma' v' J'} - E_{\gamma v J})^2 - (\omega)^2} \\ & \sum_p \begin{pmatrix} J' & 1 & J \\ -M' & -q & M \end{pmatrix}^2 \begin{pmatrix} J' & 1 & J \\ -\Omega' & -p & \Omega \end{pmatrix}^2 |\langle \gamma v|\hat{Q}_1^p|\gamma' v'\rangle|^2. \end{aligned} \tag{2.37}$$

Equation (2.37) can be separated into diagonal and non-diagonal terms with respect to γ as follows

$$\alpha_{qq}^{\gamma v J\Omega M}(\omega) = \alpha_{qq}^{rv}(\omega) + \alpha_{qq}^{ele}(\omega), \tag{2.38}$$

where

$$\alpha_{qq}^{rv}(\omega) = \sum_{v'} \sum_{J'\Omega'M'} 2(-1)^{M+M'-2\Omega}[J][J'] \frac{E_{\gamma v'J'} - E_{\gamma vJ}}{(E_{\gamma v'J'} - E_{\gamma vJ})^2 - (\omega)^2}$$
$$\sum_{p} \begin{pmatrix} J' & 1 & J \\ -M' & -q & M \end{pmatrix}^2 \begin{pmatrix} J' & 1 & J \\ -\Omega & -p & \Omega \end{pmatrix}^2 |\langle \gamma v|\hat{Q}_1^p|\gamma v'\rangle|^2, \tag{2.39}$$

and

$$\alpha_{qq}^{ele}(\omega) = \sum_{\gamma'(\neq\gamma)} \sum_{v'} \sum_{J'\Omega'M'} 2(-1)^{M+M'-\Omega-\Omega'}[J][J'] \frac{E_{\gamma' v'J'} - E_{\gamma vJ}}{(E_{\gamma' v'J'} - E_{\gamma vJ})^2 - (\omega)^2}$$
$$\sum_{p} \begin{pmatrix} J' & 1 & J \\ -M' & -q & M \end{pmatrix}^2 \begin{pmatrix} J' & 1 & J \\ -\Omega' & -p & \Omega \end{pmatrix}^2 |\langle \gamma v|\hat{Q}_1^p|\gamma' v'\rangle|^2. \tag{2.40}$$

Equation (2.39) is known as the rovibrational polarizability and corresponds to sum over the molecular states inside the same electronic curve, i.e. $\gamma' = \gamma$. Due to the symmetry properties of the $3j$-symbols, $p = 0$ thus $\Delta\Omega = 0$. $\alpha_{qq}^{rv}(\omega)$ becomes

$$\alpha_{qq}^{rv}(\omega) = \sum_{v'J'M'} (2J+1)(2J'+1) \frac{2(E_{v'J'} - E_{vJ})}{(E_{v'J'} - E_{vJ})^2 - \omega^2}$$
$$\begin{pmatrix} J' & 1 & J \\ -\Omega & 0 & \Omega \end{pmatrix}^2 \begin{pmatrix} J' & 1 & J \\ -M' & -q & M \end{pmatrix}^2 |\langle vJ|\hat{Q}_1^0|v'J'\rangle|^2, \tag{2.41}$$

where the electronic index γ has been omitted for simplicity.

Equation (2.40) accounts for the sum over different electronic states, i.e. $\gamma' \neq \gamma$, and is denoted as the electronic polarizability. This contribution $\alpha_{qq}^{ele}(\omega)$ can be separated into two terms, $p = 0$ and $p = \pm 1$. For a molecule in the electronic ground state $X^1\Sigma^+$, these are written as follows

$$\alpha_{00}(\omega) = \alpha_{\parallel}(\omega) = \sum_{\Sigma' v'} \frac{2(E_{\Sigma' v'J'} - E_{\Sigma vJ})}{(E_{\Sigma' v'J'} - E_{\Sigma vJ})^2 - (\omega)^2} |\langle \Sigma v|\hat{Q}_1^0|\Sigma' v'\rangle|^2, \tag{2.42}$$

and

$$\alpha_{\pm 1\pm 1}(\omega) = \alpha_{\perp}(\omega) = \sum_{\Pi' v'} \frac{2(E_{\Pi' v'J'} - E_{\Sigma vJ})}{(E_{\Pi' v'J'} - E_{\Sigma vJ})^2 - (\omega)^2} |\langle \Sigma v|\hat{Q}_1^{\pm 1}|\Pi' v'\rangle|^2. \tag{2.43}$$

The term $\alpha_{\parallel}(\omega)$ is the parallel electronic polarizability and involves transitions with excited electronic states with $\Omega = 0$ and $\alpha_{\perp}(\omega)$ is the perpendicular electronic polarizability, related with transition to states with $\Omega = \pm 1$ known as Π states. Using eqs. (2.42) and (2.43), the electronic

Molecule	$\alpha_{\parallel}(0)$	$\alpha_{\perp}(0)$
KRb	748.7	382.9
LiCs	597.0	262.5
LiRb	524.3	246.5
RbCs	904.0	492.3

Table 2.1: Parallel and perpendicular electronic static polarizabilities used to compute the total dynamical polarizability in eq. (2.45). Data taken from Ref. [Deiglmayr et al., 2008a].

polarizability α_{qq}^{ele} for the molecular state $|X^1\Sigma^+, v=0, J=0, M=0\rangle$ is written as

$$\alpha_{qq}^{\mathrm{el}}(\omega) = \sum_{J'M'} (2J+1)(2J'+1) \begin{pmatrix} J' & 1 & J \\ -M' & -q & M \end{pmatrix}^2 \left[\begin{pmatrix} J' & 1 & J \\ 0 & 0 & 0 \end{pmatrix}^2 \alpha_{\parallel}(\omega) + 2 \begin{pmatrix} J' & 1 & J \\ 1 & -1 & 0 \end{pmatrix}^2 \alpha_{\perp}(\omega) \right]. \tag{2.44}$$

The energy frequency of the transitions considered in eq. (2.44) are of the order of $E_{\gamma' v' J'} - E_{\Sigma v J}/\hbar \sim 10^2$ THz for alkali-diatomic molecules. Then in low frequency regime ($\omega < 5000$ GHz), $\alpha_{\parallel}(\omega)$ and $\alpha_{\perp}(\omega)$ will remain constant, thus they can be replaced by their static values $\alpha_{\parallel}(0), \alpha_{\perp}(0)$. Combining eqs. (2.41) and (2.44) (using $\alpha_{\parallel}(0), \alpha_{\perp}(0)$) into eq. (2.38), the explicit expression for the total dynamical polarizability function of the molecular state $|X^1\Sigma^+, v=0, J=0, M=0\rangle$ in the low frequency regime is given by

$$\begin{aligned} \alpha_{qq}^{JM}(\omega) = \sum_{J'M'} (2J+1)(2J'+1) \begin{pmatrix} J' & 1 & J \\ -M' & -q & M \end{pmatrix}^2 \times \\ \left[\sum_{v'} |\langle vJ| \hat{Q}_1^0 |v'J'\rangle|^2 \frac{2(E_{v'J'} - E_{vJ})}{(E_{v'J'} - E_{vJ})^2 - \omega^2} \begin{pmatrix} J' & 1 & J \\ 0 & 0 & 0 \end{pmatrix}^2 \right. \\ \left. + \begin{pmatrix} J' & 1 & J \\ 0 & 0 & 0 \end{pmatrix}^2 \alpha_{\parallel}(0) + 2 \begin{pmatrix} J' & 1 & J \\ 1 & -1 & 0 \end{pmatrix}^2 \alpha_{\perp}(0) \right], \end{aligned} \tag{2.45}$$

where we have dropped the Σ and v labels of the state notation for simplicity. The radial dipole integrals $\langle vJ| \hat{Q}_1^q |v'J'\rangle$ can be explicitly evaluated using the rovibrational wavefunctions $|vJ\rangle$ and energies E_{vJ}. We obtain $|vJ\rangle$ and E_{vJ} by solving the corresponding nuclear Schrödinger equation (i.e., vibrations plus rotations) using the Discrete Variable Representation (DVR) [Colbert and Miller, 1992]. This method requires the potential energy and the electric dipole function for the ground state $(X^1\Sigma^+, v=0, J=0)$ as a function of the internuclear distance, which are taken from Ref. [Vexiau et al., 2017] for the molecules used in this work: KRb, LiCs, LiRb and RbCs. Addicionally, the reported experimental values used for $\alpha_{\parallel}(0)$ and $\alpha_{\perp}(0)$ are tabulated in Table 2.1 as taken from Ref. [Deiglmayr et al., 2008a].

Figure 2.3 shows the dynamical polarizability for selected ground state molecules evaluated at

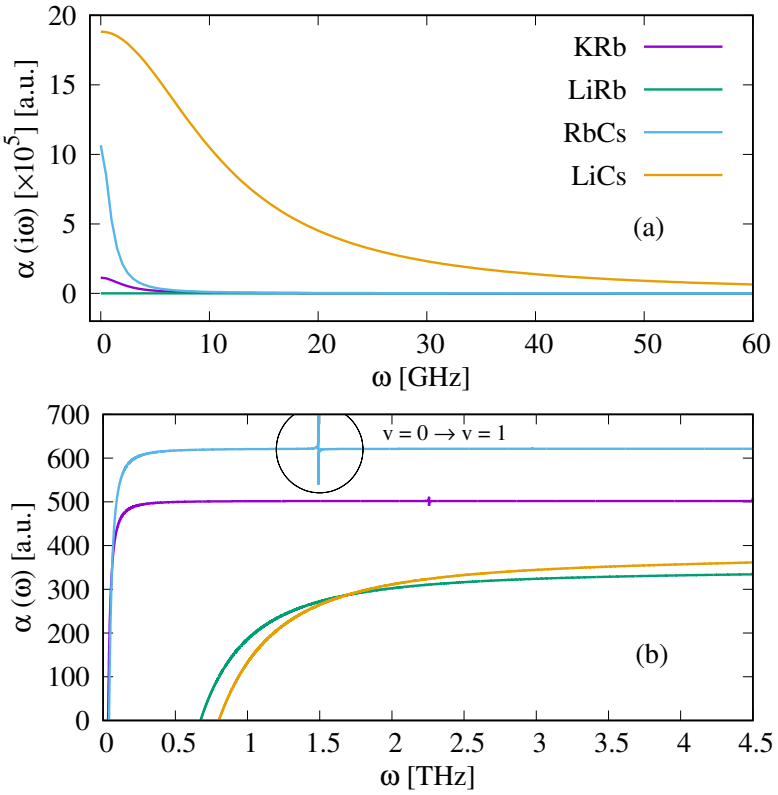

Figure 2.3: Molecular dynamical polarizability computed at (a) imaginary frequencies ($i\omega$) and (b) real frequencies (ω) using eq. (2.45) for different diatomic molecules in the electronic and rovibrational ground state $|X^1\Sigma^+, v = 0, J = 0, M = 0\rangle$. The molecular transition $v = 0 \rightarrow v = 1$ is highlighted at $\omega \approx 1.5$ THz for RbCs.

imaginary $i\omega$ and real ω frequencies up to $\omega \sim 5$ THz (KRb, RbCs, LiRb and LiCs) using eq. (2.45). At imaginary frequencies, the figure shows the decreasing monotonic character of all molecular polarizability functions studied. Whereas at real frequencies, the molecules show their characteristic resonances of the rovibrational transitions expected for $\omega < 5$ THz.

Table 2.2 compares the static values of the total polarizability (eq.(2.45)) and the electronic polarizability (eq. (2.44)) with other theoretical results. Our numerical calculation does not exceed 1% error.

As the frequency ω increases and reaches the THz regime ($\omega > 5$ THz), all molecular functions $\alpha_{qq}^{JM}(\omega)$ tend asymptotically to their isotropic static polarizabilities $\alpha_{\rm iso}^{\rm el}$, and remain constant over a large frequency range up to several hundred THz [Vexiau et al., 2017]. It was shown in Ref. [Vexiau et al., 2017], that for frequencies up to $\sim 10^3$ THz, the isotropic electronic molecular polarizability can be accurately approximated by

$$\alpha_{\rm iso}^{\rm el}(\omega) = \frac{2\omega_\Sigma\, d_\Sigma^2}{\omega_\Sigma^2 - \omega^2} + \frac{2\omega_\Pi\, d_\Pi^2}{\omega_\Pi^2 - \omega^2}, \tag{2.46}$$

where the parameters ω_Σ and d_Σ are the effective transition energy and dipole moment associated with the lowest $\Sigma \rightarrow \Sigma$ transition. The parameters ω_Π and d_Π are associated with the lowest $\Sigma \rightarrow \Pi$

Molecule	$\alpha(0)$ [Vexiau et al., 2017]	$\alpha(0)$ [This work]	$\alpha^{ele}(0)$ [Vexiau et al., 2017]	$\alpha^{ele}(0)$ [This work]
KRb	$1.141[5]$	$1.138[5]$	513.1	504.8
LiCs	$1.890[6]$	$1.890[6]$	377	374
LiRb	$9.198[5]$	$9.065[5]$	346.1	339.1
RbCs	$1.076[6]$	$1.065[6]$	621.5	629.5

Table 2.2: Total and electronic molecular static polarizabilities $(\omega = 0)$ computed using eq. (2.45) and (2.44), respectively, for molecules in a $X^1\Sigma^+$ state with $v = 0$ and $J = 0$. Our data is compared with numerical data taken from Ref. [Vexiau et al., 2017]. The square parenthesis $A[x]$ means $A \times 10^x$

transition. For the alkali-metal dimers used in this work, we use the effective parameters listed in Ref. [Vexiau et al., 2017] to estimate the electronic contribution to the molecular polarizability over the frequencies of interest.

Chapter 3

Long-range interaction between Rydberg alkali-atoms and diatomic molecules

In this Chapter, we describe the theoretical framework used to study the long-range interaction betweeen an atom and a diatomic molecule. We derive the multipolar expansion of the electrostatic interaction between two charge distributions in the spherical basis. We treat this interaction pertubartively. For ground state molecules, the first-order correction energy is zero regardless of the atomic state. The second-order correction corresponds to the van der Waals interaction energy, expressed in terms of the state-dependent dynamical polarizabities of the colliding particles.

3.1 Multipolar expansion of the electrostatic interaction

We consider two charge distributions A and B interacting through electrostatic forces that give rise to a potential energy. We assume classical point-like charges for each distribution that do not overlap with each other as shown in Fig. 3.1. The positions $\mathbf{r}_i$ ($\mathbf{r}_j$) of the charges q_i (q_j) in A (B) are given with respect to the center of mass A_C (B_C) of the distribution A (B). The vector joining A_C and B_C is denoted by $\mathbf{R}$. Without loss of generality, the center of mass A_C is fixed in the laboratory and is the origin of the coordinate frame xyz. The electrostatic potential energy V_{AB} between the two clouds in atomic units is given by

$$V_{AB} = \sum_{i\in A}\sum_{j\in B} \frac{q_i q_j}{|\mathbf{R} + \mathbf{r}_j - \mathbf{r}_i|}. \tag{3.1}$$

Since the charge clouds do not overlap, we consider them to be far away such that

$$|\mathbf{R}| \gg |\mathbf{r}_i|, |\mathbf{r}_j| \quad \forall i \in A,\ \forall j \in B. \tag{3.2}$$

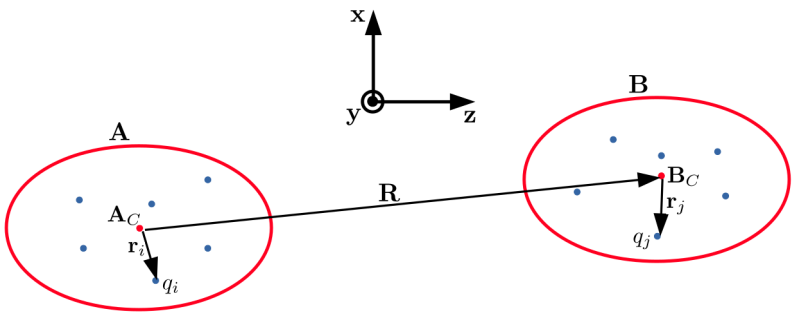

Figure 3.1: Charge distribution A and B in the xyz coordinate system.

The distance between two charges from different clouds can be written as

$$|\mathbf{R}+\mathbf{r}_j-\mathbf{r}_i| = \sqrt{(\mathbf{R}-(\mathbf{r}_i-\mathbf{r}_j))^2} = \sqrt{R^2-2\mathbf{R}\cdot\mathbf{r}_{ij}+r_{ij}^2}, \tag{3.3}$$

where $R=|\mathbf{R}|$ and the vector $\mathbf{r}_{ij}=\mathbf{r}_i-\mathbf{r}_j$ with norm $r_{ij}=|\mathbf{r}_{ij}|$. Let us denote the unit vector in $\mathbf{R}$-direction as $\hat{u}$, where $\mathbf{R}=R\hat{u}$ and the angle between the vectors $\hat{u}$ and $\mathbf{r}_{ij}$ as θ_{ij}. Equation (3.3) takes the form

$$|\mathbf{R}+\mathbf{r}_j-\mathbf{r}_i| = R\sqrt{1-\frac{2\hat{u}\cdot\mathbf{r}_{ij}}{R}+\frac{r_{ij}^2}{R^2}} = R\sqrt{1-\frac{2\mathbf{r}_{ij}\cos\theta_{ij}}{R}+\frac{r_{ij}^2}{R^2}}. \tag{3.4}$$

The reciprocal of eq. (3.4) can be expanded using the generating series of Legendre polynomials $P_L(x)$ as [Zare, 1988]

$$\frac{1}{R\sqrt{1-\frac{2\mathbf{r}_{ij}\cos\theta_{ij}}{R}+\frac{r_{ij}^2}{R^2}}} = \sum_{L=0}^{\infty}\frac{r_{ij}^L}{R^{L+1}}P_L(\cos\theta_{ij}). \tag{3.5}$$

We denote the body-fixed coordinate system as uvw, with the $\hat{u}$-axis joining the centers of mass of the distributions. If we assume that the vector $\hat{u}$ lies along the $\hat{z}$-axis, the Legendre polynomial in eq. (3.5) is proportional to the spherical harmonics $Y_L^0(\theta_{ij},\varphi_{ij})$ [Zare, 1988] where φ_{ij} is the azimuthal angle giving the orientation of $\mathbf{r}_{ij}$ in the body frame,

$$P_L(\cos\theta_{ij}) = \sqrt{\frac{4\pi}{2L+1}}Y_L^0(\theta_{ij},\varphi_{ij}). \tag{3.6}$$

Using eqs. (3.6) and (3.5), eq. (3.1) in the body-fixed frame (BF) becomes

$$V_{AB}^{BF} = \sum_{i\in A}\sum_{j\in B}\sum_{L=0}^{\infty} q_iq_j\frac{r_{ij}^L}{R^{L+1}}\sqrt{\frac{4\pi}{2L+1}}Y_L^0(\theta_{ij},\varphi_{ij}). \tag{3.7}$$

We introduce the spherical coordinates (r_i,θ_i,φ_i) of the vector $\mathbf{r}_i$ and (r_j,θ_j,φ_j) of $\mathbf{r}_j$ in the body

frame by using the following relation for the factor $r_{ij}^L Y_L^M(\theta_{ij},\varphi_{ij})$ [Varshalovich et al., 1988],

$$r_{ij}^L Y_L^M(\theta_{ij},\varphi_{ij}) = \sqrt{4\pi(2L+1)} \sum_{L_A,L_B=0}^{\infty} \delta_{L_A+L_B,L} \frac{(-1)^{L_B} r_i^{L_A} r_j^{L_B}}{\sqrt{(2L_A+1)(2L_B+1)}} \times \sum_{M_A=-L_A}^{L_A} \sum_{M_B=-L_B}^{L_B} C^{LM}_{L_AM_A,L_BM_B} Y_{L_A}^{M_A}(\theta_i,\varphi_i) Y_{L_B}^{M_B}(\theta_j,\varphi_j), \tag{3.8}$$

where $C^{LM}_{L_AM_A,L_BM_B} = \langle L_AM_A, L_BM_B | LM\rangle$ is a Clebsch-Gordan coefficient, which can be written explicitly as [Zare, 1988]

$$\langle L_AM_A, L_BM_B|LM\rangle = \delta_{M_A+M_B,M} \Bigg[(2L+1) \frac{(s-2L)!(s-2L_B)!(s-2L_A)!}{(s+1)!} \times (L_A+M_A)!(L_A-M_A)!(L_B+M_B)!(L_B-M_B)!(L+M)!(L-M)! \Bigg]^{1/2} \times \sum_{\nu} (-1)^{\nu} / \big[\nu!(L_A+L_B-L-\nu)!(L_A-M_A-\nu)!(L_B+M_B-\nu)! \times (L-L_B+M_A+\nu)!(L-L_A-M_B+\nu)! \big] \tag{3.9}$$

where $s = L_A + L_B + L$ and the index ν ranges over all integral values for which the factorial arguments are nonnegative. According to eqs. (3.7) and (3.8) $L = L_A + L_B$, therefore, the sum over ν in eq. (3.9) is restricted to $\nu = 0$ and the Clebsch-Gordan coefficient for $L = L_A + L_B$ becomes

$$C^{LM}_{L_AM_A,L_BM_B} = \sqrt{\frac{(2L_A)!(2L_B)!(L+M)!(L+M)!}{(2L)!(L_A+M_A)!(L_A-M_A)!(L_B+M_B)!(L_B-M_B)!}}. \tag{3.10}$$

Combining the relations (3.10) and (3.8) into (3.7), we find that $M = 0 \rightarrow M_A = -M_B$. Setting the variable $q = M_A = -M_B$, the final expresion for V_{AB}^{BF} reads

$$V_{AB}^{BF}(R) = \sum_{L_A=0}^{\infty} \sum_{L_B=0}^{\infty} \sum_{q=-L_<}^{L_<} \frac{f_{L_AL_Bq}}{R^{1+L_A+L_B}} Q_{L_A}^{q}(r_A) Q_{L_B}^{-q}(r_B), \tag{3.11}$$

where $L_<$ is the smallest of the integers L_A and L_B. The multipole moments $Q_{L_X}^q(\mathbf{r}_X)$ associated with a particle $X = (A, B)$ are written as

$$Q_{L_X}^q(r_X) = \left(\frac{4\pi}{2L_X+1}\right)^{1/2} \sum_i q_i r_i^{L_X} Y_{L_X}^q(\theta_i,\varphi_i). \tag{3.12}$$

Expectation values of the multipole moments depend on the electronic structure of the particle. The factor $f_{L_AL_Bq}$ in eq. (3.11) becomes

$$f_{L_AL_Bq} = \frac{(-1)^{L_B}(L_A+L_B)!}{\sqrt{(L_A+q)!(L_A-q)!(L_B+q)!(L_B-q)!}}. \tag{3.13}$$

The BF is chosen the reference frame and the superscript "BF" is dropped henceforth for simplicity.

3.2 Perturbation theory for the long-range interaction

In this Section, we consider the charge distribution A to correspond to a ground state heteronuclear diatomic molecule and the distribution B to an alkali-metal atom in a Rydberg state. In the asymptotic limit $R \to \infty$, the interaction potential V_{AB} can be treated using quantum perturbation theory [Schwabl, 2007], since the interaction energy is smaller than the transition energy between Rydberg states (ΔE_{nlj}) and the rotational transition ($\Delta E_{rot} = 2B_e$) of the molecule.

The asymptotic two-particle eigenstates can be written as

$$|\Phi_{AB}\rangle = |\Psi_A\rangle\,|\Psi_B\rangle\,, \tag{3.14}$$

where the state for the molecule is $|\Psi_A\rangle \equiv |\gamma v J\Omega M\rangle$, and the atomic state is $|\Psi_B\rangle = |n(ls)jm\rangle$. The asymptotic energy of the atom-molecule system state is given by

$$E^{(0)}_{AB} = E^{(0)}_A + E^{(0)}_B, \tag{3.15}$$

where $E^{(0)}_A \equiv E_{\gamma vJ}$ and $E^{(0)}_B \equiv E_{nlj}$.

3.2.1 First-order energy correction

The first-order correction to the two-particle energy is obtained by diagonalizing the interaction matrix $\hat{V}_{AB}$ in a given degenerate subspace $\mathcal{S} = |\gamma v J\Omega M\rangle\,|n(ls)jm\rangle$, which is $(2J+1)(2j+1)$-fold degenerate. The matrix elements $\langle\Psi'_A|\,\langle\Psi'_B|\,\hat{V}_{AB}\,|\Psi_A\rangle\,|\Psi_B\rangle$ are given by

$$\langle\Psi'_A|\,\langle\Psi'_B|\,\hat{V}_{AB}\,|\Psi_A\rangle\,|\Psi_B\rangle = \langle\gamma' v' J'\Omega' M'|\,\langle n'(l's')j'm'|\,\hat{V}_{AB}\,|n(ls)jm\rangle\,|\gamma v J\Omega M\rangle\,. \tag{3.16}$$

Inserting eq. (3.11) we explicitly have

$$\langle\Psi'_A|\,\langle\Psi'_B|\,\hat{V}_{AB}\,|\Psi_A\rangle\,|\Psi_B\rangle = \sum_{L_A=0}^{\infty}\sum_{L_B=0}^{\infty}\sum_{q=-L_<}^{L_<}\frac{f_{L_A L_B q}}{R^{1+L_A+L_B}} I_A \times I_B, \tag{3.17}$$

where

$$I_A = \langle\gamma' v' J'\Omega' M'|\,\hat{Q}^q_{L_A}(\hat{r}_A)\,|\gamma v J\Omega M\rangle\,, \tag{3.18}$$

and

$$I_B = \langle n'(l's')j'm'|\,\hat{Q}^{-q}_{L_B}(\hat{r}_B)\,|n(ls)jm\rangle\,. \tag{3.19}$$

We use angular momentum algebra to rewrite I_A and I_B in a more explicit form. As discussed in Chapter 2, Section 2.2, the molecular integral I_A can be written in a general form as

$$I_A = (-1)^{M'-\Omega'}[J']^{1/2}[J]^{1/2}\begin{pmatrix} J' & L_A & J \\ -M' & q & M \end{pmatrix} \times \sum_p \begin{pmatrix} J' & L_A & J \\ -\Omega' & p & \Omega \end{pmatrix} \langle \gamma' v'(J')| \hat{Q}^p_{L_A} |\gamma v(J)\rangle \,, \tag{3.20}$$

where $[J] = 2J + 1$.

The atomic integral I_B can be computed as in Chapter 1, Section 1.1.6 to give

$$\begin{aligned} I_B &= (-1)^{j'+j-m'+s+l}[l']^{1/2}[l]^{1/2}[j']^{1/2}[j]^{1/2} \\ &\times \begin{pmatrix} l' & L_B & l \\ 0 & 0 & 0 \end{pmatrix} \begin{pmatrix} j' & L_B & j \\ -m' & -q & m \end{pmatrix} \\ &\times \begin{Bmatrix} l & j & s \\ j' & l' & L_B \end{Bmatrix} \langle n'(l')| er^{L_B} |n(l)\rangle \,. \end{aligned} \tag{3.21}$$

Selection rules for the interaction

Let briefly recall the triangle condition that $3j$-symbol must satisfy in order to be different than zero. For a $3j$-symbol given by

$$\begin{pmatrix} j_1 & j_3 & j_2 \\ m_1 & m_3 & m_2 \end{pmatrix}, \tag{3.22}$$

$|j_1 + j_2| \geq j_3 \geq |j_1 - j_2|$ and $m_1 + m_2 + m_3 = 0$. Table 3.1 show the selection rules for different values of L_A and L_B in eqs. (3.20) and (3.21), where we have assumed that the molecule has a zero electronic angular momentum state ($\Omega = \Omega' = 0$). The $3j$-symbols from eqs. (3.20) and (3.21) define the selection rules for two given values of L_A and L_B, which determine the inverse power of atom-molecule distance in the multipole expansion (3.11).

According to Table 3.1, the diagonal elements of the interaction $\hat{V}_{AB}$ do not vanish for $L_A = L_B = 2$, giving rise to a first-order correction energy that scales as R^{-5}. We are interested in the rotational ground state ($J = J' = 0$), for which there is no first-order atom-molecule interaction because the molecules are neutral, i.e., $\langle \hat{Q}^0_{(L_A=0)} \rangle = 0$. A similar argument is valid for atoms in S states. Atom-molecule interaction for molecules in the rotational ground state (or S state atoms) would thus be expected to result in second-order corrections in the interaction potential.

The contribution of higher powers of R ($L_A, L_B > 2$) to first order in perturbation theory would not be considered because the second-order contributions associated with the polarizabilities are expected to be dominant for Rydberg atomic states.

L_A, L_B	Δl	Δj	ΔJ
$L_A = L_B = 1$	± 1	$0, \pm 1$	± 1
$L_A = 1,\ L_B = 2$	$0, \pm 2$	$0, \pm 1, \pm 2$	± 1
$L_A = 2,\ L_B = 1$	± 1	$0, \pm 1$	$0, \pm 2$
$L_A = L_B = 2$	$0, \pm 2$	$0, \pm 1, \pm 2$	$0, \pm 2$

Table 3.1: Selection rules for the angular momentum states interacting via perturbing potential $\hat{V}_{AB}$. These conditions are derived from the $3j$-symbols of eqs. (3.20) and (3.21), where we took $\Omega = \Omega' = 0$ corresponding to electronic ground state molecules.

Symmetries of the long-range potentials

From the $3j$-symbols in eqs. (3.20) and (3.21), we find that the following relations must be satisfied

$$-M' + q + M = 0, \qquad -m' - q + m = 0. \tag{3.23}$$

Therefore, we identify the following conserved quantity

$$\Omega = M + m = M' + m', \tag{3.24}$$

which characterizes the system state during the interaction. Ω is the projection of the total angular momentum $\mathbf{J}_Z = \mathbf{J}_{ZA} + \mathbf{J}_{ZB}$ of the system AB along the atom-molecule axis (not to be confused with the angular momentum projection Ω in Chapter 2).

3.2.2 Second-order energy correction

Since the first-order correction to the energy of the asymptotic state $|\Phi_{AB}\rangle = |X^1\Sigma, v = 0, J = 0, M = 0\rangle\, |n(ls)jm\rangle$ vanishes, we proceed to compute the energy correction up to a second-order. This is given by the general expression

$$E^{(2)}_{AB} = \sum_{A'B'(\neq AB)} \frac{\langle \Phi_{AB}|\hat{V}_{AB}|\Phi_{A'B'}\rangle \langle \Phi_{A'B'}|\hat{V}_{AB}|\Phi_{AB}\rangle}{(E^{(0)}_A - E^{(0)}_{A'}) + (E^{(0)}_B - E^{(0)}_{B'})}. \tag{3.25}$$

The first non-zero contribution to the second-order interaction energy is given by the dipole-dipole ($L_A = L_B = 1$) term in the multipole expansion, that is

$$\hat{V}_{AB}(R) = -\frac{2}{R^3} \sum_{q=-1}^{1} \frac{\hat{Q}^q_1(\hat{r}_A)\hat{Q}^{-q}_1(\hat{r}_B)}{\sqrt{(1+q)!(1-q)!(1+q')!(1-q')!}}, \tag{3.26}$$

which is inserted in eq. (3.25) to give

$$\begin{aligned} E^{(2)}_{AB} &= -\frac{4}{R^6} \sum_{A'B(\neq AB)} \frac{1}{(E^{(0)}_{A'} - E^{(0)}_A) + (E^{(0)}_{B'} - E^{(0)}_B)} \\ &\times \sum_{qq'} \left[\frac{\langle \Psi^{(0)}_A|\hat{Q}^q_1|\Psi^{(0)}_{A'}\rangle \langle \Psi^{(0)}_B|\hat{Q}^{-q}_1|\Psi^{(0)}_{B'}\rangle \langle \Psi^{(0)}_{A'}|\hat{Q}^{-q'}_1|\Psi^{(0)}_A\rangle \langle \Psi^{(0)}_{B'}|\hat{Q}^{q'}_1|\Psi^{(0)}_B\rangle}{(1+q)!(1-q)!(1+q')!(1-q')!} \right]. \end{aligned} \tag{3.27}$$

Equation (3.27) can be expressed as

$$E_{AB}^{(2)}(R) = \frac{C_6}{R^6}, \tag{3.28}$$

where C_6 is the dispersion coefficient, also known as van der Waals coefficient. From eq. (3.25) it can also be inferred that there are more terms to consider in eq. (3.27), i.e. $V_{AB}(R) = \sum_n \frac{C_n}{R^n}$ associated with other possibles values of L_A and L_B. However, we neglect those terms since they are expected to be small compared with the contribution of C_6.

We use the molecular state $|\Psi_A\rangle \equiv |X^1\Sigma, v = 0, J = 0, M = 0\rangle$ and the atomic state $|\Psi_B\rangle = |n(ls)jm\rangle$ in eq. (3.27) to define the products of transition dipole moments

$$\mathcal{T}_A(\gamma' v' J' M') = \langle \Sigma v J M | \hat{Q}_1^q(\hat{r}_B) | \gamma' v' J' M' \rangle \langle \gamma' v' J' M' | \hat{Q}_1^{-q'}(\hat{r}_A) | \Sigma v J M \rangle, \tag{3.29}$$

and

$$\mathcal{T}_B(n' j' l' m') = \langle n(ls)jm | \hat{Q}_1^{-q}(\hat{r}_A) | n'(l's)j'm' \rangle \langle n'(l's)j'm' | \hat{Q}_1^{q'}(\hat{r}_A) | n(ls)jm \rangle. \tag{3.30}$$

Using eqs. (3.29) and (3.30) the atom-molecule C_6 coefficient is thus given by

$$C_6 = -\sum_{qq'} \sum_{n'} \sum_{j'l'm'} \sum_{\gamma' v'} \sum_{J'M'} K(q,q') \frac{\mathcal{T}_A(\gamma' v' J' M') \mathcal{T}_B(n' j' l' m')}{(E_{n'j'l'} - E_{njl}) + (E_{\gamma' v' J'} - E_{\Sigma v J})}, \tag{3.31}$$

where $K(q,q') \equiv 4/[(1+q)!(1-q)!(1+q')!(1-q')!]$. Since the atomic and molecular transitions that contribute to the atom-molecule interaction are in the microwave frequency domain, we can restrict the summation over molecular states to rovibrational levels in the electronic ground state, such that the molecular energies can be written as E_{vJ}. Equation (3.31) thus becomes

$$C_6 = -\sum_{qq'} \sum_{n'} \sum_{j'l'm'} \sum_{v'} \sum_{J'M'} K(q,q') \frac{\mathcal{T}_A(\gamma v' J' M') \mathcal{T}_B(n' j' l' m')}{(E_{n'j'l'} - E_{njl}) + (E_{v' J'} - E_{vJ})}. \tag{3.32}$$

The C_6 dispersion coefficient can be written in a more practical form by using and alternative approach for the evaluation of summations in eq. (3.32). This approach relies on the identities

$$\frac{1}{a+b} = \frac{2}{\pi} \int_0^\infty d\omega \frac{ab}{(a^2+\omega^2)(b^2+\omega^2)}, \tag{3.33}$$

and

$$\frac{1}{a-b} = \frac{2}{\pi} \int_0^\infty d\omega \frac{ab}{(a^2+\omega^2)(b^2+\omega^2)} + \frac{2a}{a^2-b^2}, \tag{3.34}$$

which are valid for a and b positive. We identify the parameters in the identities with the transition energies from the denominators in eq. (3.32) as

$$a = E_{v' J'} - E_{vJ} \tag{3.35}$$

for molecular states. This parameter is always positive in our case since we consider the molecule

to be in the rovibrational ground state. The parameter $b > 0$ is defined as

$$b = E_{n'l'j'} - E_{nlj} \tag{3.36}$$

for upward transitions ($E_{n'l'j'} > E_{nlj}$), and

$$b = E_{nlj} - E_{n'l'j'} \tag{3.37}$$

for downward transitions ($E_{n'l'j'} < E_{nlj}$). Using these definitions it is possible to rewrite the sum-over-states in eq. (3.32) as a sum of two contributions of the form

$$\begin{aligned} C_6 \;=\; & -\sum_{q,q'} K(q,q') \Bigg[\int_0^{\omega_{\rm cut}} \frac{d\omega}{2\pi} \alpha^{nljm}_{-q-q'}(i\omega)\alpha^{JM}_{qq'}(i\omega) \\ & + \sum_{n'l'j'm'} \Theta(-\Delta E_{n'l'j'})\alpha^{JM}_{qq'}(\Delta E_{n'l'j'})\mathcal{T}_{nljm}(n'l'j'm') \Bigg], \end{aligned} \tag{3.38}$$

where $\omega_{\rm cut}$ is a cut-off frequency chosen such that the integral term converges.

The arguments of the integral in eq. (3.38) are the dynamic atomic polarizability component $\alpha^{nljm}_{-q-q'}(z)$ (see eq.(1.31)) and the dynamic molecular polarizability component $\alpha^{JM}_{qq'}(z)$ (see eq. (2.45)), each evaluated at the imaginary frequency $z = i\omega$. The second term in the square bracket represents contributions from the molecular polarizability evaluated at the real downward atomic transitions frequencies, with $\Delta E_{n'l'j'} = E_{n'l'j'} - E_{nlj}$. The Heaviside function $\Theta(x)$ enforces the downward character of the transitions that contribute to this term. These terms are weighted by the product of the atomic transition dipole integrals.

3.3 Dispersion coefficients of Rydberg alkali-atoms interacting with ground state molecules

In this Section, we use the previous approach for the analysis on the long-range interaction between two sets of collision partners: (*i*) ^{133}Cs Rydberg atoms interacting with LiCs and RbCs molecules; (*ii*) ^{85}Rb Rydberg atoms interacting with KRb, LiRb and RbCs molecules. We use eq. (3.38) to compute the C_6 coefficient of each atom-molecule pair considered, as a function of the principal quantum number n of the atomic Rydberg state $|n^2 l_j\rangle$. We restrict our calculations to atomic states with $15 \leq n \leq 150$ and $l \leq 2$.

As it was mentioned in Section 3.2.1, the total angular momentum projection along the quantization axis $\Omega = m + M$ is a conserved quantity for an atom-molecule collision. For molecules in the rovibrational ground state ($J = 0$), we have $\Omega = m$.

Following the usual convention, we have that $C_6 < 0$ defines an attractive potential, and $C_6 > 0$ defines a repulsive potential.

$n^2 l_j$	$R_{LR}(a_0)$	$R_{LR}(nm)$
$15^2P_{1/2}$	410.89	21.74
$20^2S_{1/2}$	806.23	42.66
$40^2D_{5/2}$	4452.82	235.63
$60^2P_{3/2}$	10076.97	533.25
$80^2D_{3/2}$	19006.65	1005.79

Table 3.2: LeRoy radius for several Rydberg states of a cesium atom.

The interaction length of the system is taken to be greater that the LeRoy radius [Le Roy, 1980]

$$R_{LR} = 2\left[\sqrt{\langle r_{JM}^2\rangle} + \sqrt{\langle r_{nl}^2\rangle}\right], \tag{3.39}$$

where $\langle r_{JM}^2\rangle$ and $\langle r_{nl}^2\rangle$ are the mean square length of the molecular and atomic electronic cloud, respectively. For ground state diatomic molecules, $\langle r_{JM}\rangle$ is of the order of $1-10\ a_0$, while $\langle r_{nl}\rangle$ is of the order $10^2-10^3\ a_0$ for the Rydberg states considered in this work. We can thus approximate eq. (3.39) as

$$R_{LR} \approx 2\sqrt{\langle r_{nl}^2\rangle}. \tag{3.40}$$

Since $\sqrt{\langle r_{nl}^2\rangle}$ scales as n^2, also R_{LR} does. Table 3.2 shows the values of the LeRoy radius R_{LR} using eq. (3.40) for a molecule-atom system that involves a Cs atom in a Rydberg state.

3.3.1 Cesium + Molecule

In Figure 3.2 we plot the C_6 coefficients for ^{133}Cs Rydberg states n^2l_j interacting with LiCs and RbCs molecules in the ground state $|X^1\Sigma, v=0, J=0\rangle$, as a function of the atomic principal quantum number n, for all allowed values of $|\Omega|$.

For cesium Rydberg atoms in $^2S_{1/2}$, $^2P_{1/2}$ and $^2P_{3/2}$ states (see panels (a), (b), (d), and (e) Fig. 3.2), the interaction with LiCs and RbCs ground state molecules is attractive over the entire range of n considered.

The main contribution to the C_6 coefficients comes from the integral (3.41), in which the molecular dynamical polarizability is completely positive for the ground state, therefore the attractive interaction is due to the mostly positive character of the atomic polarizability functions for the $^2S_{1/2}$, $^2P_{1/2}$ and $^2P_{3/2}$ states at imaginary frequencies $\alpha(i\omega)$.

On the other hand, Cs atoms in $^2D_{3/2}$ and $^2D_{5/2}$ Rydberg states give rise to repulsive $1/R^6$ potentials. This repulsive character of the atom-molecule interaction is due to the predominantly negative atomic polarizability function $\alpha(i\omega)$, while the molecular polarizability function remains positive.

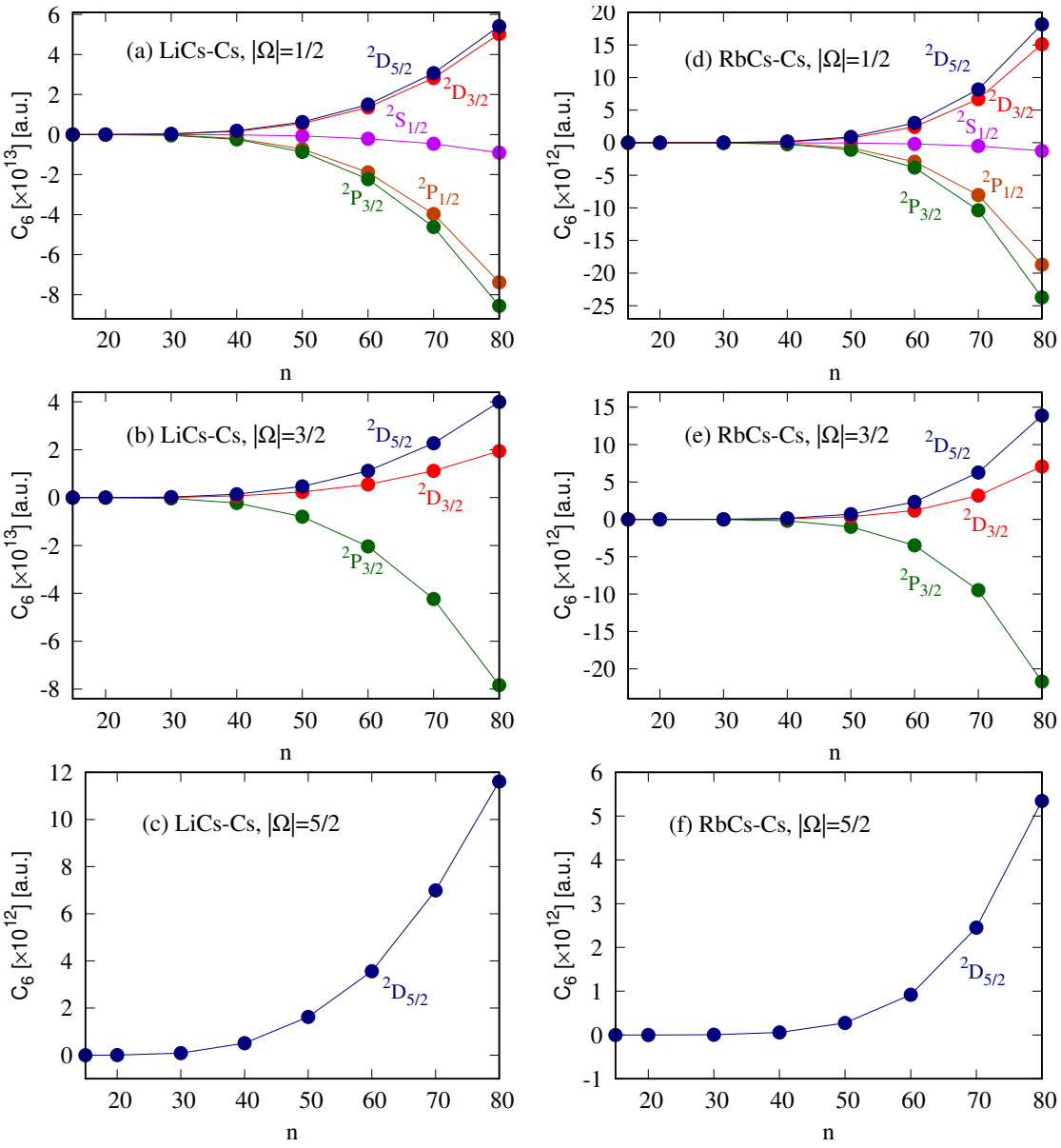

Figure 3.2: Long-range interaction coefficients C_6 as a function of the atomic principal quantum number n, using ^{133}Cs in a Rydberg state $|n^2l_j\rangle$ with (a),(b), and (c) for LiCs and (d), (e) and (f) for RbCs molecules in the electronic and rovibrational ground state $|X^1\Sigma^+\rangle\,|v=0, J=0\rangle$ for all cases. The figures are sorted by the total angular momentum projection of the system $\Omega = m + M$ along the atom-molecule axis, which is a conserved quantity through out the collision. Also, the quantum angular momentum numbers ^2l_j of the interacting atom are shown in all panels. We assume the interaction to happen at long distances ($R > R_{LR}$), where the system state can be expressed as tensor product of each particle state $|n^2l_j, m\rangle \otimes |X^1\Sigma^+ vJM\rangle$.

3.3.2 Rubidium + Molecule

In Figure 3.3 we plot the C_6 coefficients for ^{85}Rb Rydberg states $|n^2l_j\rangle$ interacting with KRb, LiCs and RbCs molecules in the rovibrational ground state, as a function of the atomic principal quantum number n, for $l \leq 2$. The C_6 coefficients for $^2S_{1/2}$, $^2P_{1/2}$ and $^2P_{3/2}$ atomic Rydberg states behave the same as interacting Cs atoms with ground state molecules, giving rise to attractive potentials. In this case, ^2D_j states do not give rise to repulsive potentials. Both, the atomic and the molecular dynamical polarizability are predominantly positive.

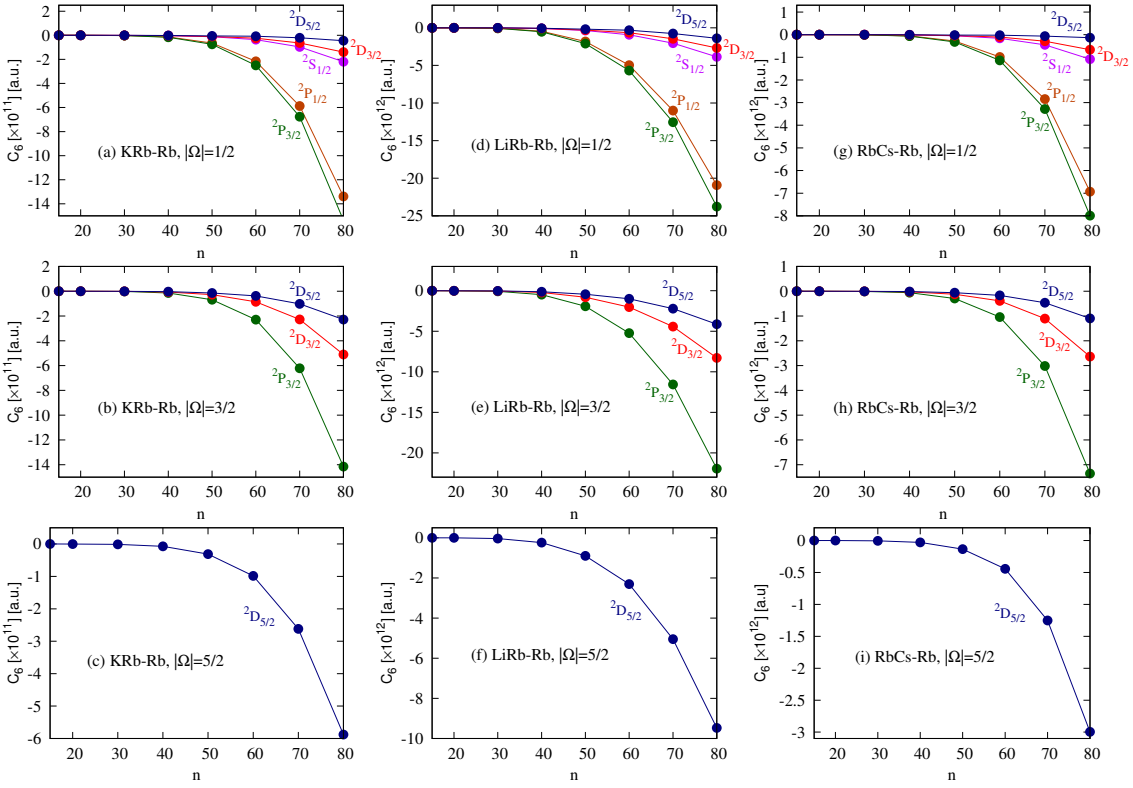

Figure 3.3: Long-range interaction coefficients C_6 as a function of the atomic principal quantum number n, using ^{85}Rb in a Rydberg state $|n^2l_j\rangle$ with (a),(b), and (c) for KRb and (d), (e), and (f) for LiRb and (g), (h), and (i) for RbCs molecules in the electronic and rovibrational ground state $|X^1\Sigma^+\rangle\,|v=0, J=0\rangle$ for all cases. The figures are sorted by the total angular momentum projection of the system $\Omega = m + M$ along the atom-molecule axis, which is a conserved quantity through out the collision. Also, the quantum angular momentum numbers ^2l_j of the interacting atom are shown in all panels. We assume the interaction to happen at long distances ($R > R_{LR}$) between the particles, where the system state can be expressed as tensor product of each particle state $|n^2l_j, m\rangle \otimes |X^1\Sigma^+ vJM\rangle$.

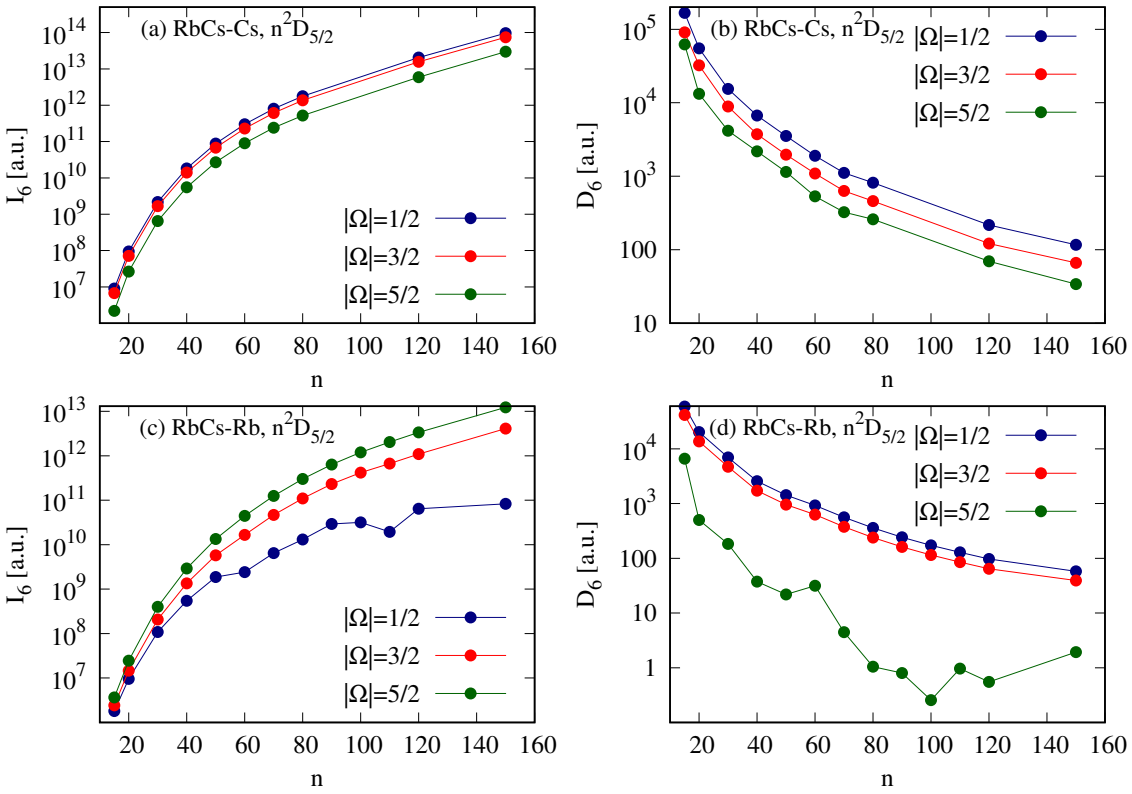

Figure 3.4: I_6 and D_6 contributions as a function of the atomic principal quantum number for (a), (b) RbCs-Cs, with the molecule in the electronic and rovibrational ground state $X^1\Sigma^+, v = 0, J = 0$ and the atom in $D_{5/2}$ state and for (c), (d) RbCs-Rb in the same molecular and atomic states. The results are presented for different total angular momentum projection Ω.

3.3.3 Frequency integral contribution

According to eq. (3.38) there are two terms that contribute to the C_6 coefficients, the integral term and the downward transitions term, given respectively by

$$I_6 = \left| \sum_{q,q'} K(q,q') \left[\int_0^{\omega_{\rm cut}} \frac{d\omega}{2\pi} \alpha^{nljm}_{-q-q'}(i\omega) \alpha^{JM}_{qq'}(i\omega) \right] \right| \tag{3.41}$$

and

$$D_6 = \left| \sum_{q,q'} \sum_{n'l'j'm'} K(q,q') \Theta(-\Delta E_{n'l'j'}) \alpha^{JM}_{qq'}(\Delta E_{n'l'j'}) \mathcal{T}_{nljm}(n'l'j'm') \right| . \tag{3.42}$$

We studied the contributions to C_6 coming from (3.41) and (3.42), separately. Figure 3.4 shows the values of the I_6 and D_6 for RbCs molecules in the ground state interacting with Cs in a ${}^2D_{5/2}$ state as a function of the atomic principal quantum number (panel (a) for I_6 and panel (b) for D_6). Panels (c) and (d) show I_6 and D_6 respectively for RbCs-Rb, with Rubidium in the atomic state ${}^2D_{5/2}$. Results are shown for different values of $|\Omega|$. Panel (d) of Figure 3.4 shows a non-monotonic behavior of D_6 as a function of n. This is due to the approximate elimination of resonant frequencies. Since D_6 involves the evaluation of the atomic transitions energy $\Delta E_{n'l'j'}$ into the

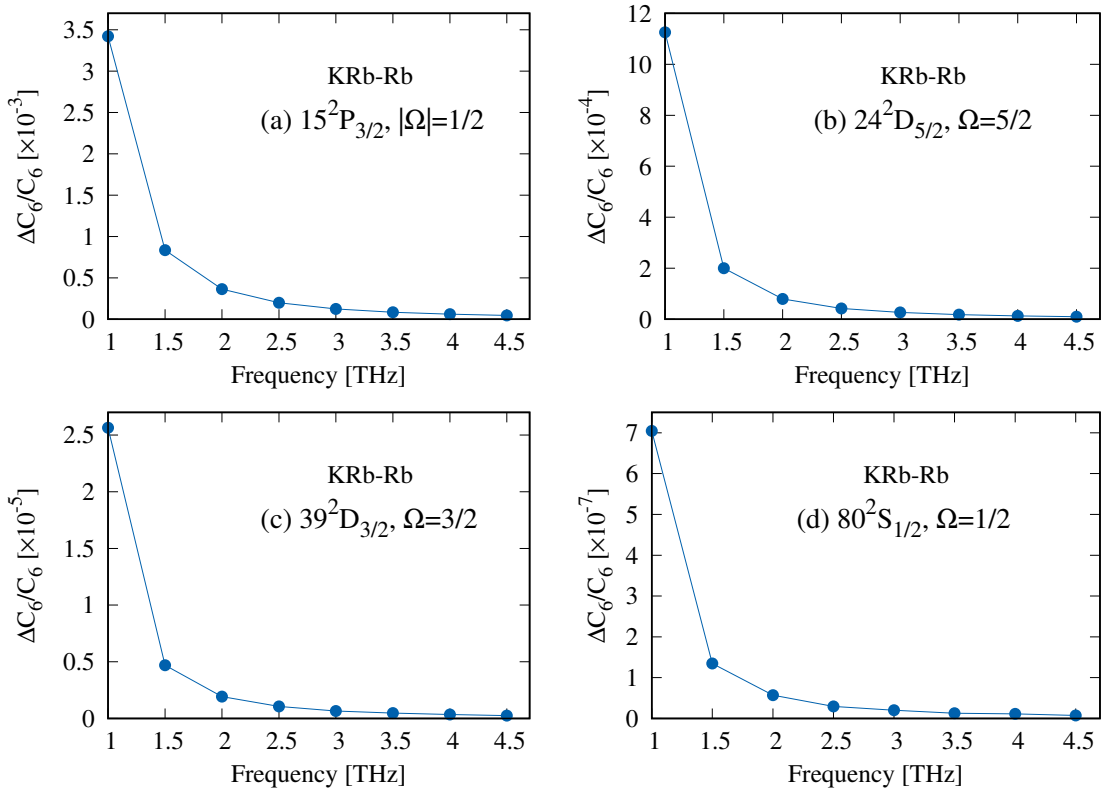

Figure 3.5: Relative change $\Delta C_6/C_6$ at different cutoff frequencies $\omega_{\rm cut}$ for a ground state KRb molecule interacting with Rubidium in a Rydberg state n^2l_j. The results are presented for different total angular momentum projection $|\Omega|$.

molecular polarizability function $\alpha_{qq'}^{JM}$, those terms which are equal to the rotational transitions in the molecule, i.e. $\Delta E_{n'l'j'} = 2B_e$, are removed from the summation of eq. (3.42). Resonant terms would contribute to the C_3 coefficients, which describe resonant energy transfer via dipole-dipole interaction between the molecule and the atom.

As n increases, the I_6 contribution becomes larger compared with the contribution of D_6 (see Fig. 3.4). The ratio of I_6/D_6 is of the order of 10^2 for $n = 15$ and reaches values of 10^{12} for $n = 150$. Therefore, the main contribution to the C_6 coefficients comes from the integral term (3.41). We find a strong dependence of C_6 on the atomic and molecular dynamical polarizability.

One way to qualitatively understand this result is to compare the n^7 scaling of the static atomic polarizability $\alpha(0)$ (related to I_6) with the n^2 scaling of the radial dipole integrals $\langle r_{nl}\rangle$ for Rydberg states (related to D_6). The ratio between I_6 (polarizability) and D_6 (dipole), in terms of n, thus scale at least as n^3.

On the other hand, both I_6 and D_6 depend on the molecular polarizability. For I_6 involving $\alpha_{qq'}^{JM}(i\omega)$, this function in the low frequency regime $\omega \leq 5$ THz is completely positive and decreases rapidly from 10^6 a.u. to 10^2 a.u. for all considered dimers (see Fig. 2.3 (a)). For D_6 involving $\alpha_{qq'}^{JM}(\omega = \Delta E_{n'l'j'})$, this function is evaluated at real frequencies with an approximate constant polarizability value of the order of 10^2 a.u. (see Fig. 2.3 (b)).

Based on the results above, we conclude that the C_6 coefficients presented here for alkali diatomic molecules in the electronic and rovibrational ground state and alkali Rydberg atoms, exhibit a strong dependence on the atomic dynamical polarizability. Therefore, mostly negative atomic polarizability functions are expected to give rise to repulsive long-range potentials, while mostly positive atomic polarizability functions would give rise to attractive potentials.

The integral I_6 involves a cut-off frequency $\omega_{\rm cut}$. In order to estimate $\omega_{\rm cut}$, we tested the numerical convergence of the integration by increasing the value of the cutoff until the relative change $\Delta C_6/C_6$ was smaller than a predefined tolerance ε. Figure 3.5 shows the results of this study. For molecule-atom pairs involving ^{133}Cs and ^{85}Rb atoms, the polarizability integral converges faster with increasing cutoff for intermediate and high values of $n \gtrsim 30$, in comparison with low-n states. The latter result in a slower convergence. We converged all our $n \approx 15$ integrals at $\omega_{\rm cut} = 3$ THz with a tolerance $\varepsilon = 0.01$, which ensures convergence over an entire range of n.

3.3.4 Scaling of C_6 with n

For both attractive and repulsive interactions, the magnitude of C_6 scales as $\sim n^7$ over a wide range of n. We fit the computed C_6 coefficients as a function of the atomic principal quantum number n to the polynomial

$$C_6 = \gamma_0 + \gamma_4\, n^4 + \gamma_6\, n^6 + \gamma_7\, n^7. \tag{3.43}$$

This scaling is valid in the range $n \approx 40 - 150$, with a fit quality that improves with increasing n. We list the fitting coefficients for Cs-LiCs and Cs-RbCs pairs in Table 3.4 for all atomic angular momentum states considered. The corresponding fitting coefficients for the collision pairs Rb-KRb, Rb-LiRb, and Rb-RbCs, are given in Table 3.5.

The n^7 scaling found for C_6 is the same scaling of the static polarizability of Rydberg atoms [Gallagher, 1994]. This suggests that the long-range interaction potential is dominated by the giant Rydberg polarizability, as expected.

Also, Table 3.3 compares the C_6 coefficients computed with eq. (3.38) and (3.43) for a ground state KRb molecule interacting with Rb atom in a $^2P_{3/2}$, with $|\Omega| = 3/2$. Equation (3.43) predicts the C_6 coefficients with an error smaller that 10% for $n > 50$.

Given the n^2 scaling of the LeRoy radius R_{LR} (3.40) and the n^7 scaling of the atom-molecule C_6 coefficients, thus, the van der Waals energy should approximately scale as $U_{\rm vdW} \equiv C_6/R_{LR}^6 \sim n^{-5}$. We find this scaling to be most accurate for $n \gtrsim 50$.

n	C_6 (Eq. 3.38)	C_6 fit (Eq. 3.43)	Error
40	-1.4476[10]	-1.4552[10]	0.007[10]
50	-6.8177[10]	-8.5246[10]	1.707[10]
60	-2.2892[11]	-2.6258[11]	0.337[11]
70	-6.2135[11]	-6.4374[11]	0.224[11]
80	-1.4146[12]	-1.3749[12]	0.040[12]
120	-1.2839[13]	-1.2843[13]	0.0004[13]
150	-4.1326[13]	-4.1326[13]	0.00005[13]

Table 3.3: Comparison of the C_6 coefficients computed using eq. (3.38) and (3.43) with the parameter shown in Table 3.5 for KRb-Rb for an atomic state $^2P_{3/2},\ |\Omega = 3/2|$. The notation $A[x]$ means $A \times 10^x$.

Molecule	l	j	$\|\Omega\|$	γ_0	γ_4	γ_6	γ_7
LiCs	S	1/2	1/2	1.518[11]	-1.035[5]	-30.94	0.1630
	P	1/2	1/2	2.104[12]	-1.984[6]	162.1	-1.606
		3/2	1/2	2.307[12]	-2.366[6]	238.2	-2.375
			3/2	2.149[12]	-2.186[6]	225.5	-2.236
	D	3/2	1/2	-1.428[12]	1.708[6]	-226.6	1.879
			3/2	-5.864[11]	7.756[5]	-134.4	1.090
		5/2	1/2	-1.431[12]	1.909[6]	-289.5	2.469
			3/2	-1.081[12]	1.462[6]	-234.1	1.973
			5/2	-3.809[11]	5.716[5]	-123.2	0.9800
RbCs	S	1/2	1/2	-2.907[10]	2.757[4]	-13.25	0.05058
	P	1/2	1/2	-3.542[11]	-1.737[5]	-3.808	-0.4723
		3/2	1/2	4.866[11]	-2.753[5]	18.15	-0.7826
			3/2	4.425[11]	-2.588[5]	19.43	-0.7408
	D	3/2	1/2	-3.906[11]	2.610[5]	-31.40	0.5847
			3/2	-2.156[11]	1.565[5]	-26.86	0.3579
		5/2	1/2	-4.818[11]	3.501[5]	-53.47	0.8316
			3/2	-3.846[11]	2.821[5]	-45.57	0.6657
			5/2	-1.901[11]	1.458[5]	-29.63	-0.3334

Table 3.4: Parameters for the fitting $C_6 = \gamma_0 + \gamma_4\, n^4 + \gamma_6\, n^6 + \gamma_7\, n^7$, for selected atom-molecule pairs involving ^{133}Cs atoms in Rydberg states $|n^2 l_j\rangle$, interacting with LiCs and RbCs molecules in the ground electronic and rovibrational state. $\Omega = m$ is the total angular momentum projection of the collision pair. C_6 is in atomic units (a_0^3). The fitting is accurate in the range $n = 40 - 150$. The notation $A[x]$ means $A \times 10^x$.

Molecule	l	j	$\|\Omega\|$	γ_0	γ_4	γ_6	γ_7
KRb	S	1/2	1/2	4.340[9]	-1905	-0.5274	4.695[-4]
	P	1/2	1/2	1.155[10]	27.48	-6.706	0.02190
		3/2	1/2	1.429[10]	-840.9	-7.419	0.02381
			3/2	1.227[10]	9.555	-7.089	0.02286
	D	3/2	1/2	4.907[9]	-3284	0.1596	-1.883[-3]
			3/2	6.531[9]	-2307	-2.039	6.199[-3]
		5/2	1/2	3.298[9]	-2486	0.4228	-2.302[-3]
			3/2	4.481[9]	-2337	-0.5691	1.173[-3]
			5/2	6.782[9]	-2026	-2.521	8.018[-3]
LiRb	S	1/2	1/2	1.381[11]	-1.085[5]	6.408	-0.04418
	P	1/2	1/2	5.353[11]	-4.224[5]	-13.06	0.01194
		3/2	1/2	6.063[11]	-4.839[5]	-12.77	1.718[-3]
			3/2	5.598[11]	-4.420[5]	-14.57	0.01386
	D	3/2	1/2	1.091[11]	-1.040[5]	11.58	-0.06377
			3/2	2.100[11]	-2.024[5]	3.214	-0.03349
		5/2	1/2	8.086[10]	-7.309[4]	10.89	-0.05510
			3/2	1.317[11]	-1.237[5]	7.670	-0.04539
			5/2	2.309[11]	-2.225[5]	1.254	-0.02591
RbCs	S	1/2	1/2	1.316[10]	-3897	-2.743	-7.242[-3]
	P	1/2	1/2	-1.576[10]	5.049[4]	-39.63	0.07148
		3/2	1/2	-1.225[10]	5.381[4]	-44.40	0.07713
			3/2	-1.640[10]	5.347[4]	-41.94	0.07316
	D	3/2	1/2	2.285[10]	-1.490[4]	1.265	-0.01663
			3/2	9.039[9]	7469	-12.55	0.01839
		5/2	3/2	5.808[10]	-1.796[4]	-1.099	-0.01126
			5/2	5.978[10]	-2261	-13.17	0.01667

Table 3.5: Parameters for the fitting $C_6 = \gamma_0 + \gamma_4\, n^4 + \gamma_6\, n^6 + \gamma_7\, n^7$, for selected atom-molecule pairs involving ^{85}Rb atoms in Rydberg states $|n^2 l_j\rangle$, interacting with RbCs, LiRb and KRb molecules in the ground electronic and rovibrational state. $\Omega = \mathrm{m}$ is the total angular momentum projection of the collision pair. C_6 is in atomic units (a_0^3). The fitting is accurate in the range $n = 40 - 150$. The notation $A[x]$ means $A \times 10^x$.

3.3.5 Error bounds on C_6 values

There are two terms that must be considered in order to estimate the accuracy of the frequency integral in eq. (3.38) which has the major contribution to the van der Waals coefficients as we explaneid in Section 3.3.3. The first one is the the molecular dynamical polarizability and the second one is the atomic dynamical polarizability of a Rydberg state.

The rovibrational structure and electrostatic response of most alkali-metal dimers in the ground $X^1\Sigma$ state is well-known from precision spectroscopy experiments and accurate *ab-initio* studies [Deiglmayr et al., 2008a, Deiglmayr et al., 2008b, Deiglmayr et al., 2011]. Therefore, the molecular polarizability function α_{qq}^{JM} in eq. (2.45) is assumed to be known with very high precision, our computed static molecular polarizabilities differ from the results in Ref. [Vexiau et al., 2017] by less than 1%, as we showed in Chapter 2. These polarizability functions evaluated at imaginary frequencies $\alpha_{qq}^{JM}(i\omega)$ is always positive and have their maximum value at $\omega = 0$, as the frequency increses the polarizabilities tend asymptotically to their isotropic static values $\alpha_{\rm iso}^{\rm el}$ for each considered molecule. Therefore the molecular polarizabilities are bounded from above by their static value.

For the atomic Rydberg states considered, the polarizability functions obtained from eq. (1.31) are predominantly monotonic as a function of frequency, although we found specific states $|n^2 l_j, m\rangle$ with non-monotonic frequency dependence (see Chapter 2). Again, the maximum absolut value of the atomic polarizability at imaginary frequencies occur when $\omega = 0$. For higher frequencies the polarizability increses or decreses, depending on the atomic states, and tends to an asymptotic value up to a cutoff frequency $\omega_{\rm cut}$ of a few THz. In general, for all the atomic states considered, we find that $|\alpha_{qq}^{nljm}(i\omega)|$ is always bounded from above by its value at $\omega = 0$.

The accuracy of our computed atomic polarizability functions $\alpha_{qq}^{nljm}(i\omega)$ is limited by the precision of the quantum defects used, which we take from spectroscopic measurements [Singer, 2004].

The error of the computed C_6 coefficients can thus be estimated for $n \geq 15$ as follows. Ignoring the downward transition terms (D_6), and the error in the molecular polarizability function, equation (3.38) can be written as $\tilde{C}_6 = C_6 \pm \delta C_6$, where $\tilde{C}_6$ is the dispersion coefficient obtained in our calculations, and the error is approximately given by

$$\delta C_6 \approx -\sum_{q,q'} \frac{K(q,q')}{2\pi} \int_0^{\omega_{\rm cut}} \frac{d\omega}{2\pi}\, \delta\alpha_{qq'}^{nljm}(i\omega)\, \alpha_{-q-q'}^{JM}(i\omega), \tag{3.44}$$

where $\delta\alpha_{qq'}^{nljm}(i\omega)$ is the error in the atomic polarizability function evaluated at imaginary frequencies. The order of magnitude of the product integral $\int \alpha_{qq'}^{nljm}(i\omega)\alpha_{-q-q'}^{JM}(i\omega)$ is the same for all qq'-components, we can thus assume that the relative error $\delta\alpha_{qq}^{nljm}(i\omega)/\alpha_{qq}^{nljm}(i\omega)$ is the same for all qq'-components and remains constant over all frequencies up to the cutoff $\omega_{\rm cut}$. We use the fact that $|\alpha(i\omega)|$ is bounded from above by its static value in the atomic and molecular cases, we can estimate an approximate error bound for C_6 in terms of the relative error of the 00-component as

$$\left|\frac{\delta C_6}{C_6}\right| \lesssim \left|\frac{\delta\alpha_{00}^{nljm}(0)}{\alpha_{00}^{nljm}(0)}\right|. \tag{3.45}$$

In other words, the accuracy of our C_6 calculations can not expected to be better than the accuracy of the static atomic polarizability. The static polarizabilities of several Rydberg states of ^{85}Rb and ^{133}Cs are known from laser spectroscopy measurements in static electric fields [Zimmerman et al., 1979, O'Sullivan and Stoicheff, 1986, Zhao et al., 2011], and also from precision calculations using state-of-the-art *ab-initio* pseudo-potentials [Yerokhin et al., 2016]. Therefore, we estimated $\delta\alpha_{00}^{nljm}(0)$ for several atomic Rydberg states $|n^2l_j, m\rangle$, by comparing with available data (see Table 1.8). The average relative errors for Rb is -0.02% for $^2S_{1/2}$ states over the range $15 \leq n \leq 50$ for $^2S_{1/2}$ states, $+0.27\,\%$ for $^2D_{5/2}$ states with $m = 5/2$, and $+0.13\,\%$ for $^2D_{3/2}$ states with $m = 3/2$. Similar accuracies are obtained for Cs.

Another possible source of error in our C_6 calculations is the choice of the high frequency cutoff $\omega_{\rm cut}$ in the numerical integration of eq. (3.38).

3.3.6 Effect of the molecular dipole moment

In Figure 3.6 we show the increase in the magnitude of C_6 as the permanent dipole moment of alkali-metal dimers increases, for selected states $n^2P_{1/2}$ of ^{85}Rb. The C_6 coefficient for the Rb-LiRb pair is larger than the corresponding values for RbCs and KRb, which have a smaller dipole moment. The same trend also holds for other $|n^2l_j\rangle$ states of ^{85}Rb, and for atom-molecule pairs involving ^{133}Cs atoms.

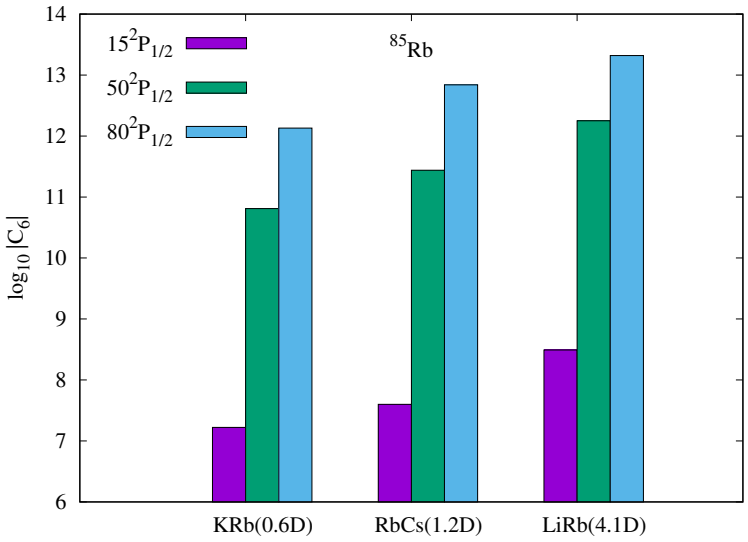

Figure 3.6: Bar plots $\log_{10}|C_6|$ for $n = 15, 50, 80$ for atom-molecule pairs involving ^{85}Rb atoms in the $n^2P_{1/2}$ state with KRb, RbCs and LiRb molecules in the rovibrational ground state. The permanent dipole moment of each molecule is shown in parenthesis on the horizontal axis [Deiglmayr et al., 2008a].

Conclusions

In this Thesis, we theoretically study the long-range interaction between Rydberg alkali-atoms and diatomic molecules. The interaction potential in the molecule-Rydberg system at large distances is small compared with the internal energy of each particle, therefore it is treated using quantum pertubation theory and given in terms of the atomic and molecular dynamical polarizability functions. We study ^{133}Cs and ^{85}Rb atoms in a Rydberg state $|n^2l_j, m\rangle$ with $l \leq 2$ and $15 < n < 150$ interacting with KRb, LiCs, LiRb and RbCs molecules in the electronic and rovibrational ground state $|X^1\Sigma^+, v = 0, J = 0, M = 0\rangle$. For this molecular state the interaction is determined by the C_6 van der Waals coefficient and the interaction scales in terms of the particles relative distance as C_6/R^6. We found that the atomic polarizabilty function evaluated at imaginary frequencies $i\omega$ has a crucial role in the interaction: determines the magnitude and the nature of the interaction, i.e. whether it is attractive ($C_6 < 0$) or repulsive ($C_6 > 0$).

We also found that the interaction is not only determined by atomic properties and quantum numbers, the interacting molecule may enhance the interaction according to its permanent dipole moment, i.e. polar molecules with higher permanent dipole moment experience a stronger interaction compare with molecules with smaller permanent dipole moment, assuming that both are interacting with the same atomic species and in the same atomic quantum state. Therefore, it is possible to find an atomic Rydberg state and a molecule that gives an attractive or repulsive potential with a desired interaction strength.

Repulsive van der Waals interactions may be used for sympathetic cooling of alkali-metal dimers via elastic collisions with ultracold Rydberg atoms. For example, for the LiCs-Cs system with ^{133}Cs in the $n^2D_{5/2}$ state and $|\Omega = 5/2|$, the van der Waals potential is repulsive (Fig. 3.2(c)) and can be estimated in absolute units with a collisional barrier reaching $U_{\rm vdW} \approx 38$ MHz for $n = 20$. This should be sufficient to avoid short-range collisions for atom-molecule pairs with relative kinetic energy up to 1.82 mK. By increasing the atomic quantum number to $n = 40$, the potential barrier drops to $U_{vdW} \approx 0.43$ MHz for the same collision pair. Since inelastic and reactive ultracold collisions [Julienne, 2009, Idziaszek and Julienne, 2010] can lead to spontaneously emitted photons carrying energy away from a trapped system [Zhao et al., 2012], it should be possible to measure the elastic-to-inelastic scattering rates and follow the thermalization process of a co-trapped atom-molecule mixture.

Attractive van der Waals potentials can be exploited to form long-range alkali-metal trimers via photoassociation [Shaffer et al., 2018]. Using eq. (1) from Chapter , we can extend the long-range

potential to the short-range by setting $R_0 = C_6$ and compute the system wavefunction in the whole range, by finding the Franck-Condon overlap [Condon, 1926, Franck and Dymond, 1926] between two system states, we can estimate the photoassociation rates.

We can extend the formalism in this work to also obtain van der Waals coefficients for excited rovibrational states of alkali-metal dimers. In this case, C_5 coefficients do not vanish in general [Lepers et al., 2010]. The interplay between C_5 and C_6 with opposite signs at long distances can possibly lead to long-range potential wells that can support Rydberg-like metastable bound states accessible in photoassociation spectroscopy [Lepers and Dulieu, 2011, Lepers et al., 2011, Lepers et al., 2010, Pérez-Ríos et al., 2015].

Bibliography

[Amaldi and Segrè, 1934] Amaldi, E. and Segrè, E. (1934). Effetto della pressione sui termini elevati degli alcalini. *Il Nuovo Cimento*, 11(145).

[Bellos et al., 2013] Bellos, M. A., Carollo, R., Banerjee, J., Eyler, E. E., Gould, P. L., and Stwalley, W. C. (2013). Excitation of weakly bound molecules to trilobitelike rydberg states. *Phys. Rev. Lett.*, 111:053001.

[Bendkowsky et al., 2009] Bendkowsky, V., Butscher, B., Nipper, J., Shaffer, J. P., Löw, R., and Pfau, T. (2009). Observation of ultralong-range rydberg molecules. *Nature*, 458:1005–1008.

[Bethe and Salpeter, 1957] Bethe, H. A. and Salpeter, E. A. (1957). *Quantum Mechanics of One and Two Electron Atoms*. Academic Press.

[Bhatti et al., 1981] Bhatti, S. A., Cromer, C. L., and Cooke, W. E. (1981). Analysis of the rydberg character of the $5d7d^1d_2$ state of barium. *Phys. Rev. A*, 24:161–165.

[Blasing et al., 2016] Blasing, D. B., Stevenson, I. C., Pérez-Ríos, J., Elliott, D. S., and Chen, Y. P. (2016). Short-range photoassociation of lirb. *Phys. Rev. A*, 94:062504.

[Bonin and Kresin, 1997] Bonin, K. D. and Kresin, V. V. (1997). *Electric-dipole polarizabilities of atoms, molecules and clusters*. World Scientific Publising.

[Booth et al., 2015] Booth, D., Rittenhouse, S. T., Yang, J., Sadeghpour, H. R., and Shaffer, J. P. (2015). Production of trilobite rydberg molecule dimers with kilo-debye permanent electric dipole moments. *Science*, 348(6230):99–102.

[Born and Oppenheimer, 1927] Born, M. and Oppenheimer, R. (1927). Zur quantentheorie der molekeln. *Annalen der Physik*, 389(20):457–484.

[Brown and Carrington, 2003] Brown, J. and Carrington, A. (2003). *Rotational spectroscopy of diatomic molecules*. Cambridge University Press.

[Carr et al., 2009] Carr, L. D., DeMille, D., Krems, R. V., and Ye, J. (2009). Cold and ultracold molecules: science, technology and applications. *New Journal of Physics*, 11(5):055049.

[Colbert and Miller, 1992] Colbert, D. T. and Miller, W. H. (1992). A novel discrete variable representation for quantum mechanical reactive scattering via the s-matrix kohn method. *The Journal of Chemical Physics*, 96(3):1982–1991.

[Condon, 1926] Condon, E. (1926). A theory of intensity distribution in band systems. *Phys. Rev.*, 28:1182–1201.

[Debye, 1920] Debye, P. (1920). *Zeitschrift für Physik*, 21.

[Deiglmayr et al., 2008a] Deiglmayr, J., Aymar, M., Wester, R., Weidemuller, M., and Dulieu, O. (2008a). Calculations of static dipole polarizabilities of alkali dimers: Prospects for alignment of ultracold molecules. *The Journal of Chemical Physics*, 129(6):064309.

[Deiglmayr et al., 2008b] Deiglmayr, J., Grochola, A., Repp, M., Mortlbauer, K., Gluck, C., Lange, J., Dulieu, O., Wester, R., and Weidemuller, M. (2008b). Formation of ultracold polar molecules in the rovibrational ground state. *Phys. Rev. Lett.*, 101(13):133004–4.

[Deiglmayr et al., 2016] Deiglmayr, J., Herburger, H., Saßmannshausen, H., Jansen, P., Schmutz, H., and Merkt, F. (2016). Precision measurement of the ionization energy of cs i. *Phys. Rev. A*, 93:013424.

[Deiglmayr et al., 2011] Deiglmayr, J., Repp, M., Wester, R., Dulieu, O., and Weidemüller, M. (2011). Inelastic collisions of ultracold polar lics molecules with caesium atoms in an optical dipole trap. *Phys. Chem. Chem. Phys.*, 13:19101–19105.

[Dunham, 1932] Dunham, J. L. (1932). The energy levels of a rotating vibrator. *Phys. Rev.*, 41:721–731.

[Fermi, 1934] Fermi, E. (1934). Sopra lo spostamento per pressione delle righe elevate delle serie spettrali. *Il Nuovo Cimento*, 11(157).

[Franck and Dymond, 1926] Franck, J. and Dymond, E. G. (1926). Elementary processes of photochemical reactions. *Trans. Faraday Soc.*, 21:536–542.

[Gallagher, 1994] Gallagher, T. F. (1994). *Rydberg atoms*. Cambridge University Press.

[Greene et al., 2000] Greene, C. H., Dickinson, A. S., and Sadeghpour, H. R. (2000). Creation of polar and nonpolar ultra-long-range rydberg molecules. *Phys. Rev. Lett.*, 85:2458–2461.

[Herrera, 2012] Herrera, F. (2012). *PhD Thesis: Quantum control of binary and many-body interactions in ultracold molecular gases*. University of British Columbia.

[Huber and Büchler, 2012] Huber, S. D. and Büchler, H. P. (2012). Dipole-interaction-mediated laser cooling of polar molecules to ultracold temperatures. *Phys. Rev. Lett.*, 108:193006.

[Idziaszek and Julienne, 2010] Idziaszek, Z. and Julienne, P. S. (2010). Universal rate constants for reactive collisions of ultracold molecules. *Phys. Rev. Lett.*, 104:113202.

[Jaksch et al., 2000] Jaksch, D., Cirac, J. I., Zoller, P., Rolston, S. L., Côté, R., and Lukin, M. D. (2000). Fast quantum gates for neutral atoms. *Phys. Rev. Lett.*, 85:2208–2211.

[Jarisch and Zeppenfeld, 2018] Jarisch, F. and Zeppenfeld, M. (2018). State resolved investigation of förster resonant energy transfer in collisions between polar molecules and rydberg atoms. *New Journal of Physics*, 20(11):113044.

[Jones and Chapman, 1924] Jones, J. E. and Chapman, S. (1924). On the determination of molecular fields ii. from the equation of state of a gas. *Proceedings of the Royal Society of London. Series A, Containing Papers of a Mathematical and Physical Character*, 106(738):463–477.

[Jones et al., 2006] Jones, K. M., Tiesinga, E., Lett, P. D., and Julienne, P. S. (2006). Ultracold photoassociation spectroscopy: Long-range molecules and atomic scattering. *Rev. Mod. Phys.*, 78:483–535.

[Julienne, 2009] Julienne, P. S. (2009). Ultracold molecules from ultracold atoms: a case study with the krb molecule. *Faraday Discuss.*, 142:361–388.

[Kamenski et al., 2017] Kamenski, A. A., Manakov, N. L., Mokhnenko, S. N., and Ovsiannikov, V. D. (2017). Energy of van der waals and dipole-dipole interactions between atoms in rydberg states. *Phys. Rev. A*, 96:032716.

[Keesom, 1921] Keesom, W. (1921). *Zeitschrift für Physik*, 22.

[Lai et al., 2018] Lai, Z., Zhang, S., Gou, Q., and Li, Y. (2018). Polarizabilities of rydberg states of rb atoms with n up to 140. *Phys. Rev. A*, 98:052503.

[Le Roy, 1980] Le Roy, R. J. (1980). Theory of deviations from the limiting near-dissociation behavior of diatomic molecules. *The Journal of Chemical Physics*, 73(12):6003–6012.

[Lebedev, 1965] Lebedev, N. N. (1965). *Special functions and their applications*. Prentice-Hall.

[Lei et al., 1995] Lei, T., Gu, S., Weng, Z., and Zeng, X. (1995). Measurement of the polarizabilities of n^2d rydberg states of cesium. *Zeitschrift für Physik D Atoms, Molecules and Clusters*, 34:139–141.

[Lepers and Dulieu, 2011] Lepers, M. and Dulieu, O. (2011). Long-range interactions between ultracold atoms and molecules including atomic spin–orbit. *Phys. Chem. Chem. Phys.*, 13:19106–19113.

[Lepers and Dulieu, 2017] Lepers, M. and Dulieu, O. (2017). Long-range interactions between ultracold atoms and molecules.

[Lepers et al., 2010] Lepers, M., Dulieu, O., and Kokoouline, V. (2010). Photoassociation of a cold-atom–molecule pair: Long-range quadrupole-quadrupole interactions. *Phys. Rev. A*, 82:042711.

[Lepers et al., 2011] Lepers, M., Vexiau, R., Bouloufa, N., Dulieu, O., and Kokoouline, V. (2011). Photoassociation of a cold-atom-molecule pair. ii. second-order perturbation approach. *Phys. Rev. A*, 83:042707.

[L'Huillier et al., 1982] L'Huillier, A., Lompre, L. A., Mainfray, G., and Manus, C. (1982). Multiply charged ions formed by multiphoton absorption processes in the continuum. *Phys. Rev. Lett.*, 48:1814–1817.

[Li et al., 2003] Li, W., Mourachko, I., Noel, M. W., and Gallagher, T. F. (2003). Millimeter-wave spectroscopy of cold rb rydberg atoms in a magneto-optical trap: Quantum defects of the ns, np, and nd series. *Phys. Rev. A*, 67:052502.

[Liebisch et al., 2016] Liebisch, T. C., Schlagmüller, M., Engel, F., Nguyen, H., Balewski, J., Lochead, G., Böttcher, F., Westphal, K. M., Kleinbach, K. S., Schmid, T., Gaj, A., Löw, R., Hofferberth, S., Pfau, T., Pérez-Ríos, J., and Greene, C. H. (2016). Controlling rydberg atom excitations in dense background gases. *Journal of Physics B: Atomic, Molecular and Optical Physics*, 49(18):182001.

[Liveing and Dewar, 1879] Liveing, G. D. and Dewar, J. (1879). V. on the spectra of sodium and potassium. *Proceedings of the Royal Society of London*, 29(196-199):398–402.

[London, 1930] London, F. (1930). Zur theorie und systematik der molekularkräfte. *Zeitschrift für Physik*, 63.

[Lukin et al., 2001] Lukin, M. D., Fleischhauer, M., Cote, R., Duan, L. M., Jaksch, D., Cirac, J. I., and Zoller, P. (2001). Dipole blockade and quantum information processing in mesoscopic atomic ensembles. *Phys. Rev. Lett.*, 87:037901.

[Marinescu et al., 1994] Marinescu, M., Sadeghpour, H. R., and Dalgarno, A. (1994). Dispersion coefficients for alkali-metal dimers. *Phys. Rev. A*, 49:982–988.

[Molony et al., 2014] Molony, P. K., Gregory, P. D., Ji, Z., Lu, B., Köppinger, M. P., Le Sueur, C. R., Blackley, C. L., Hutson, J. M., and Cornish, S. L. (2014). Creation of ultracold $^{87}\mathrm{Rb}^{133}\mathrm{Cs}$ molecules in the rovibrational ground state. *Phys. Rev. Lett.*, 113:255301.

[Ni et al., 2008] Ni, K.-K., Ospelkaus, S., de Miranda, M. H. G., Pe'er, A., Neyenhuis, B., Zirbel, J. J., Kotochigova, S., Julienne, P. S., Jin, D. S., and Ye, J. (2008). A high phase-space-density gas of polar molecules. *Science*, 322(5899):231–235.

[Ni et al., 2010] Ni, K.-K., Ospelkaus, S., Wang, D., Quéméner, G., Neyenhuis, B., de Miranda, M. H. G., Bohn, J. L., Ye, J., and Jin, D. S. (2010). Dipolar collisions of polar molecules in the quantum regimes. *Nature*, 464:1324–1328.

[Numerov, 1927] Numerov, B. (1927). Note on the numerical integration of $d^2x/dt^2 = f(x, t)$. *Astronomische Nachrichten*, 230(19):359–364.

[O'Sullivan and Stoicheff, 1986] O'Sullivan, M. S. and Stoicheff, B. P. (1986). Scalar and tensor polarizabilities of ^2d rydberg states in rb. *Phys. Rev. A*, 33:1640–1645.

[P. and P., 1967] P., D. and P., R. (1967). *Methods of Numerical Integration*. Blaisdell Publishing.

[Pérez-Ríos et al., 2015] Pérez-Ríos, J., Lepers, M., and Dulieu, O. (2015). Theory of long-range ultracold atom-molecule photoassociation. *Phys. Rev. Lett.*, 115:073201.

[Rydberg, 1890] Rydberg, J. R. (1890). Xxxiv. on the structure of the line-spectra of the chemical elements. *The London, Edinburgh, and Dublin Philosophical Magazine and Journal of Science*, 29(179):331–337.

[Samboy et al., 2011] Samboy, N., Stanojevic, J., and Côté, R. (2011). Formation and properties of rydberg macrodimers. *Phys. Rev. A*, 83:050501.

[Schwabl, 2007] Schwabl, F. (2007). *Quantum Mechanics*. Springer-Verlag Berlin Heidelberg.

[Schäfer, 1990] Schäfer, F. P. (1990). *Dye Lasers*. Springer-Verlag Berlin Heidelberg.

[Shaffer et al., 2018] Shaffer, J. P., Rittenhouse, S. T., and Sadeghpour, H. R. (2018). Ultracold rydberg molecules. *Nature Communications*, 9(1):1965.

[Singer, 2004] Singer, K. (2004). *PhD Thesis: Interactions in an ultracold gas of Rydberg atoms*. University of Freiburg.

[Varshalovich et al., 1988] Varshalovich, D. A., Moskalev, A. N., and Khersonskii, V. K. (1988). *Quantum Theory of Angular Momentum*. World Scientific Publishing.

[Vexiau et al., 2017] Vexiau, R., Borsalino, D., Lepers, M., Orbán, A., Aymar, M., Dulieu, O., and Bouloufa-Maafa, N. (2017). Dynamic dipole polarizabilities of heteronuclear alkali dimers: optical response, trapping and control of ultracold molecules. *International Reviews in Physical Chemistry*, 36(4):709–750.

[Wang, 2014] Wang, T. T. (2014). *PhD thesis: Small Diatomic Alkali Molecules at Ultracold Temperatures*. Harvard University.

[White, 1934] White, H. E. (1934). *Introduction to Atomic Spectra*. McGraw-Hill.

[Yerokhin et al., 2016] Yerokhin, V. A., Buhmann, S. Y., Fritzsche, S., and Surzhykov, A. (2016). Electric dipole polarizabilities of rydberg states of alkali-metal atoms. *Phys. Rev. A*, 94:032503.

[Zare, 1988] Zare, R. N. (1988). *Angular Momentum*. John Wiley & Sons.

[Zeppenfeld, 2017] Zeppenfeld, M. (2017). Nondestructive detection of polar molecules via rydberg atoms. *EPL*, 118(1):13002.

[Zhao et al., 2012] Zhao, B., Glaetzle, A. W., Pupillo, G., and Zoller, P. (2012). Atomic rydberg reservoirs for polar molecules. *Phys. Rev. Lett.*, 108:193007.

[Zhao et al., 2011] Zhao, J., Zhang, H., Feng, Z., Zhu, X., Zhang, L., Li, C., and Jia, S. (2011). Measurement of polarizability of cesium nd state in magneto-optical trap. *Journal of the Physical Society of Japan*, 80(3):034303.

[Zimmerman et al., 1979] Zimmerman, M. L., Littman, M. G., Kash, M. M., and Kleppner, D. (1979). Stark structure of the rydberg states of alkali-metal atoms. *Phys. Rev. A*, 20:2251–2275.

Appendix A

Numerov algorithm

In this Appendix we derive the Numerov algorithm, which is designed to numerically solve ordinary differential equations of the form

$$\frac{d^2y(x)}{dx^2} + k^2(x)y(x) = 0. \tag{A.1}$$

We start by applying the operator $1 + \frac{h^2}{12}\frac{d^2}{dx^2}$ (h is a very small number) into eq. (A.1) to obtain

$$\frac{h^2}{12}y^{(4)} + y^{(2)} + \frac{h^2}{12}\frac{d^2}{dx^2}\left[k^2(x)y(x)\right] + k^2y(x) = 0, \tag{A.2}$$

where $y^{(n)} \equiv \frac{d^n y(x)}{dx^n}$. Expanding $y(x+h)$ and $y(x-h)$ in Taylor series around h and $-h$, respectively,

$$y(x+h) = y(x) + hy^{(1)}(x) + \frac{h^2}{2!}y^{(2)}(x) + \frac{h^3}{3!}y^{(3)}(x) + \frac{h^4}{4!}y^{(4)}(x) + ..., \tag{A.3}$$

and

$$y(x-h) = y(x) - hy^{(1)}(x) + \frac{h^2}{2!}y^{(2)}(x) - \frac{h^3}{3!}y^{(3)}(x) + \frac{h^4}{4!}y^{(4)}(x) + ... \tag{A.4}$$

Adding $y(x+h)$ and $y(x-h)$,

$$y(x+h) + y(x-h) = 2y(x) + h^2y^{(2)}(x) + \frac{h^2}{12}y^{(4)}(x), \tag{A.5}$$

and solving for $y^{(2)}$, we obtain

$$y^{(2)}(x) = \frac{y(x+h) + y(x-h) - 2y(x)}{h^2} - \frac{h^2}{12}y^{(4)}(x). \tag{A.6}$$

We replace eq. (A.6) into (A.2) to obtain

$$\frac{y(x+h) + y(x-h) - 2y(x)}{h^2} + \frac{h^2}{12}\frac{d^2}{dx^2}\left[k^2(x)y(x)\right] + k^2y(x) = 0. \tag{A.7}$$

The expression $\frac{d^2}{dx^2}\left[k^2(x)y(x)\right]$ can be approximate using the derivative definition given by

$$\frac{d}{dx}\left[k^2(x)y(x)\right] \approx \frac{k^2(x+h)y(x+h) - k^2(x)y(x)}{h}, \tag{A.8}$$

explicitly,

$$\frac{d^2}{dx^2}\left[k^2(x)y(x)\right] \approx \frac{\frac{k^2(x+h)y(x+h)-k^2(x)y(x)}{h} - \frac{k^2(x)y(x)-k^2(x-h)y(x-h)}{h}}{h}, \tag{A.9}$$

$$\frac{d^2}{dx^2}\left[k^2(x)y(x)\right] \approx \frac{k^2(x+h)y(x+h) - 2k^2(x)y(x) + k^2(x-h)y(x-h)}{h^2}. \tag{A.10}$$

Replacing eq. (A.10) into (A.7) and solving for $y(x+h)$, we obtain

$$y(x+h) = \frac{y(x)\left[2 - \frac{5h^2}{6}k^2(x)\right] - y(x-h)\left[1 + \frac{h^2}{12}k^2(x-h)\right]}{1 + \frac{h^2}{12}k^2(x+h)}. \tag{A.11}$$

If we label de continuos variable x as a discrete one as j, then equation (A.11) becomes

$$y_{j+h} = \frac{2y_j\left[1 - \frac{5h^2}{12}k_j^2\right] - y_{j-h}\left[1 + \frac{h^2}{12}k_{j-h}^2\right]}{1 + \frac{h^2}{12}k_{j+h}^2}. \tag{A.12}$$

According to eq. (A.12), this algorithm requires to know the values of y_0 and y_1 to move forward through the lattice, or know the values at last lattice sites y_{N-1} and y_N to move backwards through the lattice.

Appendix B

Dynamical polarizability function

In this Appendix a detailed derivation of the dynamical polarizability function is provided for a general polarizable system. The polarizability is found by considering the lowest order correction to the electric-dipole moment of the system [Bonin and Kresin, 1997].

Let $\psi_k^{(0)}$ for $k = 1, 2, 3...$ be the eigenfunctions of the unperturbed Hamiltonian $\hat{H}_0$ that satisfies the time-independent Schrodinger equation

$$\hat{H}_0\psi_k^{(0)} = E_k^{(0)}\psi_k^{(0)}, \tag{B.1}$$

where $E_k^{(0)}$ is the unperturbed energy corresponding to the k-th state.

Supose that we apply a time-dependent perturbing Hamiltonian $\hat{H}_I(t)$ given by

$$\hat{H}_I(t) = \hat{V}e^{i\omega t} + h.c., \tag{B.2}$$

where $h.c.$ is the Hermitian conjugate and the operator $\hat{V}$ is given by

$$\hat{V} = -\frac{1}{2}\hat{\mathbf{p}} \cdot \mathbf{E}_0, \tag{B.3}$$

where $\hat{\mathbf{p}}$ is the quantum dipole moment operator given by

$$\hat{\mathbf{p}} = \sum_i q_i\hat{\mathbf{r}}_i, \tag{B.4}$$

where q_i is the charge of the i-th particle in the system at the $\hat{\mathbf{r}}_i$ position. Considering a time-dependent electric field oscillating with frequency ω and form

$$\mathbf{E}(t) = \mathbf{E}_0e^{-i\omega t} + \mathbf{E}_0^{\dagger}e^{i\omega t}. \tag{B.5}$$

where $\mathbf{E}_0$ is the vector amplitude that contains the polarization of the field.

Let us consider the system to be initially in the quantum state k and the perturbing Hamiltonian

couples the inicial state with the state l. We can write the system wavefuncion in a general way as

$$\phi(t) = a_k(t)\psi_k^{(0)} e^{-iE_k^{(0)}t/\hbar} + a_l(t)\psi_l^{(0)} e^{-iE_l^{(0)}t/\hbar} \tag{B.6}$$

where a_k, a_l are chosen in such a way that they satisfy the Schrodinger equation

$$i\hbar\frac{\partial}{\partial t}\phi(t) = \left[\hat{H}_0 + \hat{H}_I\right]\phi(t). \tag{B.7}$$

Replacing eq. (B.6) into (B.7), we obtain

$$\begin{aligned} i\hbar\dot{a}_k\psi_k^{(0)} e^{-iE_k^{(0)}t/\hbar} + i\hbar\dot{a}_l\psi_l^{(0)} e^{-iE_l^{(0)}t/\hbar} = \\ a_k\hat{H}_I\psi_k e^{-iE_k^{(0)}t/\hbar} + a_l\hat{H}_I\psi_l e^{-iE_l^{(0)}t/\hbar}, \end{aligned} \tag{B.8}$$

where $\dot{a}_k \equiv \frac{d}{dt}a_k$ and we have omitted the time-dependency of the coefficients a_k, a_l for simplicity. Multipling the equation (B.8) by $\psi_l^{*(0)} e^{iE_l^{(0)}t/\hbar}$ from the left and integrating over the spacial coordinates, equation (B.8) becomes

$$i\hbar\dot{a}_l(t) = a_k(t)\left[V_{lk}e^{i(\omega_{lk}-\omega)t} + V_{lk}^{\dagger}e^{i(\omega_{lk}+\omega)t}\right] \tag{B.9}$$

where $w_{lk} = \left(E_l^{(0)} - E_k^{(0)}\right)/\hbar$ and V_{lk} is a matrix element of the perturbing potential, explicitly

$$V_{lk} = \int \psi_l^{*(0)}\hat{V}\psi_k^{(0)} d^3\mathbf{r}, \tag{B.10}$$

where $d^3\mathbf{r}$ is the volume element. We had assumed in eq. (B.9) that the diagonal elements of the interaction Hamiltonian are zero, i.e. $V_{kk} = 0$. Equation (B.9) can be integrated assuming that the amplitude $a_k(t)$ varies much slower than the oscillating frequency $\omega_{lk} \pm \omega$ at the interval $[t_0, t]$, where $|a_l(t_0)| = 0$ and $|a_k(t_0)| = 1$. Therefore, the solution for the amplitude $a_l(t)$ becomes

$$a_l(t) = -a_k(t_0)\left[\frac{V_{lk}(e^{i(\omega_{lk}-\omega)t} - e^{i(\omega_{lk}-\omega)t_0})}{\hbar(\omega_{lk}-\omega)} + \frac{V_{lk}^{\dagger}(e^{i(\omega_{lk}+\omega)t} - e^{i(\omega_{lk}+\omega)t_0})}{\hbar(\omega_{lk}+\omega)}\right]. \tag{B.11}$$

Let us consider a general operator $\hat{G}$ that is time-independent, using the general system state $\phi(t)$, we compute the matrix element of $\hat{G}$ as

$$\int\left[\phi^*\hat{G}\phi\right]d^3\mathbf{r} = |a_k|^2G_{kk} + a_k^*a_lG_{kl}e^{-i\omega_{lk}t} + a_ka_l^*G_{lk}e^{i\omega_{lk}t} + |a_l|^2G_{ll}, \tag{B.12}$$

where

$$G_{kl} = \int \psi_k^{*(0)}\hat{G}\psi_l^{(0)} d^3\mathbf{r}. \tag{B.13}$$

is time-independent. The first term on the right hand side of equation (B.12) is the zeroth-order correction of the operator and is independent of the perturbing potential (B.2). The last term is second-order in the perturbing Hamiltonian (involving $|a_l|^2$). The two intermediate terms are the first-order correction of $\hat{G}$, in which we are interested. We can replace eq. (B.11) into (B.12) keeping only the first-order correction, making $|a_k(t)| = |a_k(t_0)| = 1$ and retaining only the harmonic

terms ωt, equation (B.12) to the first-order thus becomes

$$\left[\int \phi^* \hat{G} \phi d^3\mathbf{r}\right]^{(1)} = -\left[e^{-i\omega t}\left(\frac{V_{lk}G_{kl}}{\hbar(\omega_{lk}-\omega)} + \frac{V_{kl}G_{lk}}{\hbar(\omega_{lk}+\omega)}\right) + e^{i\omega t}\left(\frac{V^*_{kl}G_{kl}}{\hbar(\omega_{lk}+\omega)} + \frac{V^*_{lk}G_{lk}}{\hbar(\omega_{lk}-\omega)}\right)\right]. \tag{B.14}$$

We briefly recall the time-independent perturbation theory [Schwabl, 2007] in order to obtain expression of the static polarizability.

The energy correction of the k-th state under a perturbing potential $\hat{V}$ is given by

$$E_k = E_k^{(0)} + V_{kk} + \sum_{l(\neq k)} \frac{|V_{kl}|^2}{E_k^{(0)} - E_l^{(0)}} + ..., \tag{B.15}$$

We focus on the second-order correction term of the energy and using eq. (B.3), thus equation (B.15) is written as

$$E_k^{(2)} = \sum_{l(\neq k)} \frac{\hat{\mathbf{p}}^*_{kl}\hat{\mathbf{p}}_{lk}}{E_k^{(0)} - E_l^{(0)}}\mathbf{E}_0^2. \tag{B.16}$$

Or using the well-known expression

$$E_k^{(2)} = -\frac{1}{2}\alpha\mathbf{E}_0^2 \tag{B.17}$$

where α is the static polarizability given by

$$\alpha = 2\sum_{l(\neq k)} \frac{\hat{\mathbf{p}}^*_{kl}\hat{\mathbf{p}}_{lk}}{E_l^{(0)} - E_k^{(0)}}. \tag{B.18}$$

We must consider an external electric field $\mathbf{E}$ of the form (B.5) in order to obtain the explicit expression of the frequency-dependent polarizability, which is defined by only considering the first-order correction to the diagonal matrix element of the dipole operator [Bonin and Kresin, 1997]. Therefore, for an harmonic external electric field the induced dipole moment is written as

$$\hat{\mathbf{p}}^{(1)}_{kk}(t) = \frac{1}{2}\left[\hat{\mathbf{p}}_{kk}e^{-i\omega t} + c.c.\right], \tag{B.19}$$

where $c.c.$ is the complex conjugate of previous expression. The diagonal matrix element of the i-th component of the electric dipole moment operator is related to the polarizability tensor by [Bonin and Kresin, 1997]

$$(\hat{\mathbf{p}}_i)_{kk} = (\hat{\alpha}_{ij})_{kk}(\omega)(\mathbf{E}_0)_j, \tag{B.20}$$

where $(\hat{\alpha}_{ij})_{kk}(\omega)$ is the ij-th component of the polarizability tensor at frequency ω for a system in the k-th state. If we take the electric dipole moment operator $\hat{\mathbf{p}}_i$ instead of $\hat{G}$ and replace $\hat{V} = (1/2)\hat{\mathbf{p}}\cdot\mathbf{E}_0$ in eq. (B.14), the first-order correction of the dipole moment becomes

$$(\hat{\mathbf{p}}_i)^{(1)}_{kk} = \frac{1}{2}\sum_{l(\neq k)}\left[e^{-i\omega t}\left(\frac{(\hat{p}_i)_{kl}(\hat{p}_j)_{lk}(E_0)_j}{\hbar(\omega_{lk}-\omega)} + \frac{(\hat{p}_i)_{lk}(\hat{p}_j)_{kl}(E_0)_j}{\hbar(\omega_{lk}+\omega)}\right)\right.$$
$$\left. + e^{i\omega t}\left(\frac{(\hat{p}_i)_{kl}(\hat{p}_j)^*_{kl}(E_0)^*_j}{\hbar(\omega_{lk}+\omega)} + \frac{(\hat{p}_i)_{lk}(\hat{p}_j)^*_{lk}(E_0)^*_j}{\hbar(\omega_{lk}-\omega)}\right)\right]. \tag{B.21}$$

The sum over l in eq. (B.21) is the general expression of (B.14) considering that the perturbing

Hamiltonian couples the state k with several quantum states [Bonin and Kresin, 1997]. Comparing eq. (B.21) with eqs. (B.20) and (B.19), the ij-th component of the polarizability tensor at frequency ω for a system in the k-th state is given by

$$(\hat{\alpha}_{ij})_{kk}(\omega) = \sum_{l(\neq k)} \left[\frac{(\hat{p}_i)_{kl}(\hat{p}_j)_{lk}}{\hbar(\omega_{lk} - \omega)} + \frac{(\hat{p}_i)_{lk}(\hat{p}_j)_{kl}}{\hbar(\omega_{lk} + \omega)} \right]. \tag{B.22}$$

Since the matrix elements of the electric dipole operator are real, i.e. $(\hat{p}_j)^*_{kl} = (\hat{p}_j)_{kl}$, and for convenience of the angular momentum states used in this Thesis $\psi_k \equiv |k\rangle$, we can write the dipole moment operator using the spherical tensor operators as $\hat{p}_q \equiv \hat{Q}^q_1$, where $(\hat{Q}^q_1)^\dagger = (-1)^{-q}\hat{Q}^{-q}_1$. The final expression for the dynamical polarizability is written as,

$$(\hat{\alpha}_{qq'})_{kk}(\omega) = 2(-1)^q \sum_{l(\neq k)} \frac{E^{(0)}_l - E^{(0)}_k}{\left(E^{(0)}_l - E^{(0)}_k\right)^2 - \omega^2} \langle k|\hat{Q}^q_1|l\rangle \langle l|\hat{Q}^{-q'}_1|k\rangle, \tag{B.23}$$

where we had used qq' instead of ij.